# ANALYTICAL-BASED METHODOLOGIES FOR MONITORING THE UPTAKE, DISTRIBUTION AND MOLECULAR INTERACTION OF SILVER NANOPARTICLES WITH HUMAN RED BLOOD CELLS

A thesis submitted in partial fulfillment of the

requirements for the degree of

Master of Science

By

KELSEY L. HOOD

B.S., Thomas More College, 2016

2018

Wright State University

WRIGHT STATE UNIVERSITY

GRADUATE SCHOOL

August 2rd, 2018

I HEREBY RECOMMEND THAT THE THESIS PREPARED UNDER MY SUPERVISION BY Kelsey L. Hood ENTITLED Analytical-Based Methodologies for Monitoring the Uptake, Distribution and Molecular Interaction of Silver Nanoparticles with Human Red Blood Cells BE ACCEPTED IN PARTIAL FULFILLMENT OF THE REQUIREMENTS FOR THE DEGREE OF Master of Science.

_____

Ioana E. Pavel, Ph.D.
Thesis Director

_____

David A. Grossie, Ph.D.
Chair, Department of Chemistry

Committee on

Final Examination

_____

Ioana E. Pavel, Ph.D.

_____

David A. Dolson, Ph.D.

_____

Norma Adragna, Ph.D.

_____

Barry Milligan, Ph.D.
Interim Dean of Graduate School

## ABSTRACT

Hood, Kelsey L. M.S. Department of Chemistry, Wright State University, 2018. Analytical-Based Methodologies for Monitoring the Uptake, Distribution and Molecular Interaction of Silver Nanoparticles with Human Red Blood Cells

The production and incorporation of silver nanoparticles into consumer products and biomedical technologies has skyrocketed in recent years. Thus, it is vital that the uptake, distribution and molecular interaction of silver nanoparticles (AgNPs) with red blood cells is well studied. In this experiment, citrate capped AgNPs 5-10 nm in diameter were incubated with washed red blood cells in a 5% glucose solution for one hour. Unbound AgNPs were removed via glucose washes prior to quantification with graphite furnace atomic absorption spectroscopy and analysis via Cytoviva hyperspectral microscopy and Raman spectroscopy. It was determined that a high percentage of 48±5% of AgNPs were taken up by the cells. Approximately 70% of the AgNPs taken up were adhered to the cell membrane and the rest were found within the cells. Obvious membrane damage was observed in many of these cells. Hyperspectral data showed interaction of extracellular and intracellular AgNPs with cholesterol, phospholipids or other cell membrane components, and hemoglobin respectively. The intracellular interaction with hemoglobin was confirmed by the enhancement of characteristic hemoglobin Raman shifts. Diminished oxyhemoglobin peaks and enhanced deoxyhemoglobin peaks revealed that the AgNP exposed cells showed a decrease in oxygen binding which could have been a result of intracellular and/or extracellular AgNP interactions. After 24 hours of storage at 4°C, SERS enhancement of >400% proved extracellular AgNPs aggregated forming large clusters of cells. In addition to the proven toxicity of silver ions, the adverse effects

seen in the results of this study show that exposure of AgNPs to the circulatory system could pose serious health concerns.

# Table of Contents

# List of Figures

# List of Tables

# List of Schemes

## ACKNOWLEDGEMENTS

First and foremost, I would like to thank God for the amazing opportunities and strength he has given me over the last two years; I could not have gotten this degree without him. I would also like to thank Dr. Ioana Pavel for her guidance and support during my graduate research. The positive light and dedication that she brings to her research and students is admirable. Next, I would like to express gratitude to my committee members, Dr. Adragna and Dr. Dolson, for their advice and input on this research. I would like to thank the chemistry department at WSU for the opportunity to further develop my passion for teaching while pursuing this degree. I am so grateful for my colleagues in Dr. Pavel's research group for everything from assistance in lab to keeping me sane these past two years. My friends and family deserve special thanks for their continued support and love during this difficult process.

# 1. INTRODUCTION

## 1.1 Importance of Silver Nanoparticles

Nanoparticle incorporation into everyday consumer products is a new and booming engineering tactic. In addition to being lighter in weight, materials can increase in reactivity, electrical conductance and mechanical properties with the integration of nanoparticles.[1] The revenue from engineered nanomaterials has seen a consistent increase since these products have been on the market. In 2013, the United States revenue was $318 billion and the worldwide revenue was $1 trillion.[2] Consumers are buying goods without the knowledge that they contain nanoparticles, because manufacturers are not currently required to advertise or register their products as utilizing nanotechnology.[3] The Project on Emerging Nanotechnologies created an inventory that lists suspected and known consumer products that contain nanoparticles of all sorts.[1] There are thousands of everyday products on this list including bed sheets, clothing, cookware, toothpaste, makeup, lawn treatments and even children's toys. Figure 1.1 shows the different categories into which the products fall, and the most popular nanomaterials used. Nanoparticles are used most often in health and fitness products, with the majority of these products being ingested or placed in direct contact with skin. It can

also be seen that silver is most abundantly used in nanoproducts on the market today due to its antimicrobial properties.

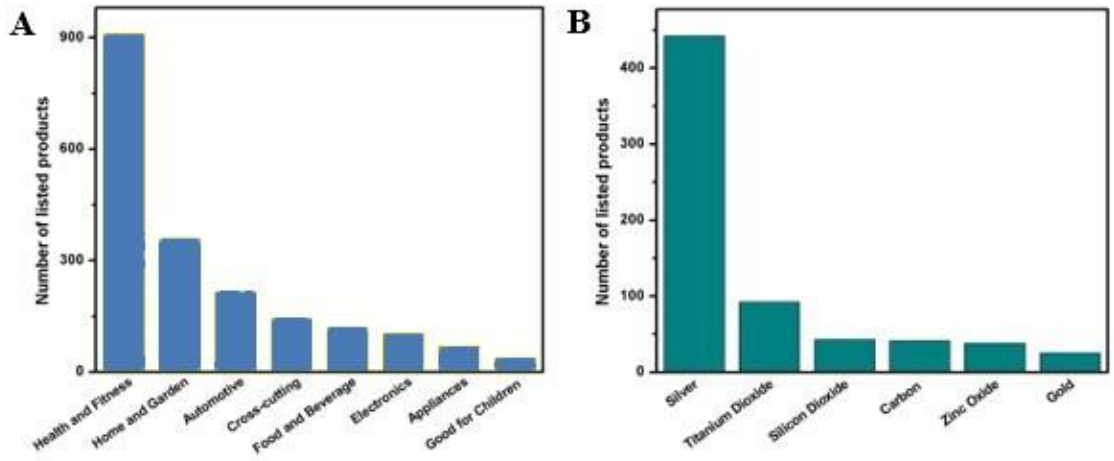


**Figure 1.1** Total number of consumer products containing nanomaterials by A) category and B) type of nanomaterial. (Charts constructed by Kelsey Hood using data from the Consumer Products Inventory)[1]

Not only are silver nanoparticles (AgNPs) commonly used in everyday consumer products, they are also widely used in biomedical devices. Because of their antibacterial properties, AgNPs have been used in wound gels, bandages, catheters, cardiovascular implants and bone cements.[4] It should be noted that it is not the nanoparticles themselves, but rather the silver ions that are released from the nanoparticles over time that are killing the bacteria. The rate at which ionic silver is released from the nanoparticles can be controlled by changing the size, coating and matrix in which the nanoparticles are dispersed.[5] Additionally, recent studies have found that AgNPs have anti-inflammatory and antiviral properties, though the inhibition mechanisms are not yet well understood.[4, 6] AgNPs also exhibit unique optical properties which make them of use as biosensing agents in cancer detection and Alzheimer's.[7, 8] Experimental chemotherapies and other localized drug delivery techniques have begun to incorporate AgNPs.[9, 10] Due to the

antibacterial, antiviral, anti-inflammatory, anti-cancer and optical properties of AgNPs, their biomedical applications are essentially limitless. Many of these upcoming uses and technologies will put AgNPs in direct contact with the cardiovascular and central nervous systems.

## 1.2 Synthesis and Properties of Silver Nanoparticles

There are countless techniques for synthesizing AgNPs, but each synthesis falls into one of two categories: top-down or bottom-up. Top-down synthesis methods start with a large, bulk material that is broken down into particles on the nanometer ($10^{-9}$ m) scale. Included in top-down processes are laser ablation, electro-explosion, photolithography and anodization.[11, 12] This type of process is typically used in industry to quickly synthesize large quantities of nanomaterials. Bottom-up processes are the opposite in that atoms or molecules are brought together to build nanoparticles. Examples would be reduction, precipitation, plasma spraying synthesis, chemical vapor deposition (CVD), chemical vapor condensation (CVC) and self-assembly.[13] Bottom-up processes, especially reduction of silver salts, allow more opportunities for size and shape selectivity and tailoring of the nanoparticles for specific uses.

The general chemical reaction scheme (Scheme 1.1) for the synthesis of AgNP via reduction can be seen below. Silver ions are reduced and conglomerate to form silver nanoparticles. The particles can further be coated or stabilized with a plethora of ions or molecules.


**Scheme 1.1** Generalized synthetic scheme for coated silver nanoparticles.

Silver (I) has a positive reduction potential of 0.799 V in water, therefore a reducing agent must be used. The most common reducing agents are sodium borohydride ($E^0$= -0.481 V), sodium citrate ($E^0$= -0.180 V), hydrazine ($E^0$= -0.230 V) and hydroquinone ($E^0$= -0.699 V).[14] Borohydride and citrate are also popular capping agents along with polyethylene glycol (PEG) and L-lysine.[12, 15] PEG and lysine capped AgNPs have a positive surface charge, while borohydride and citrate are negatively charged. All four capping agents are considered biocompatible.[16]

The physical and chemical characteristics (PCCs) of nanoparticles that the EPA deems important are size, morphology, surface area, chemical composition, solubility, surface chemistry and reactivity related to the coating, as well as the conductive, magnetic and optical properties.[17] While these characteristics determine nanoparticles' fate in the environment, they also affect the nanoparticles effectiveness in the engineered, biomedical or industrial applications, along with their toxicity. Size, morphology, surface area and composition can all be controlled during synthesis, but the reactivity, conductivity, magnetic and optical properties are results of the synthesis.

The most popular synthesis methods are Lee-Meisel (citrate capped) and Creighton (borohydride capped).[18, 19] Lee-Meisel is a very robust synthesis that uses

sodium citrate as both the reducing agent and the capping agent and produces large (>50 nm), spherical nanoparticles. The concentrations, volumes and time scale used in the reaction can be modified to produce nanoparticles of different sizes and shapes. Once a colloid is synthesized, the PCCs must be determined through characterization.

Common colloid characterization techniques include UV-visible light absorption spectroscopy (UV-VIS), Raman spectroscopy, and inductively coupled plasma-optical emission spectroscopy (ICP-OES). These techniques provide information about the size, size distribution, purity and concentration of the colloid. UV-VIS measures the light that is absorbed during the excitation of the localized surface plasmon resonance which is a cloud of free electrons surrounding the surface of the nanoparticle. Citrate capped silver nanoparticles around 5-10 nm in diameter have been shown to exhibit a surface plasmon resonance peak with a maximum around 390 nm.[20, 21, 22] Raman spectroscopy uses a laser to excite the vibrational and rotational transitions of chemical bonds to test the purity of a colloid. A pure colloid would reveal only Raman shifts for the liquid in which the nanoparticles are dispersed, typically water. Metallic nanoparticles are often used for surface enhanced Raman spectroscopy (SERS). The nanoparticles are surrounded by an electric field which can be enhanced via excitation of the surface plasmon (electron gas) at the metals surface. The enhancement of the local electric field enhances the Raman modes in the surrounding molecules which leads to the enhanced Raman signal.

### 1.3 Toxicity of Silver Nanoparticles

A massive amount of research has proven that silver nanoparticles have antimicrobial properties which is the reason for their incorporation into health and fitness, and biomedical products.[22, 23, 24] However, the toxicity and long-term effects of exposure

to silver nanoparticles are not as well known. Several studies have assessed the toxicity of silver nanoparticles *in vitro* and *in vivo.*

*In vitro* studies have shown the production of reactive oxygen species (ROS) in various cell lines including human lung epithelial adenocarcinoma (A549), human lung fibroblasts (IMR-90) and human glioblastoma cells (U251l), when exposed to AgNPs for short periods of time.[25, 26, 27] ROS in high concentrations can have adverse effects on cells including damage to DNA, enzymes, lipids, amino acids in proteins, necrosis and apoptosis.[28] DNA can be further damaged by silver ions which are released from AgNPs over time.[29] Other studies have shown that AgNPs inhibit mitochondrial activity in murine hippocampal neuronal (HT22) cells and macrophage cells (RAW 264.7).[30, 31] The genotoxicity and cytotoxicity are largely affected by the surface chemistry, concentration and size of the AgNPs. In general, smaller NPs in high concentrations enter cells more readily, thus increasing toxic effects.[32]

While many *in vitro* studies have demonstrated the toxicity of AgNPs, significantly less research has been done *in vivo*. Experiments on rats have shown accumulation and damage to the liver and brain.[33, 34] In one study, AgNPs caused an unexplained decrease in platelet aggregation in mice.[35] Investigation on the effects of AgNPs on embryonic zebrafish showed slowed development, increased mortality rates and higher toxicity than silver nitrate.[36, 37] Both *in vivo* and *in vitro* studies have proven AgNPs can have cytotoxic and damaging effects to major organs, the circulatory system, DNA, mitochondria and proteins. There is a desperate need for *in vivo* research to further determine the effects of long term exposure and bioaccumulation in organisms.

## 1.4 Background on Red Blood Cells

Red blood cells (RBCs) have a vital role in our bodies as they carry and deliver oxygen to tissues and major organs. RBCs contain a high concentration of hemoglobin, 7-11 mmol/L, which gives them their red color. Hemoglobin is a quaternary protein in which each subunit contains a heme group. The porphyrin ring forms a special kind of covalent bond called a coordinate bond with $Fe^{2+}$ which acts as the binding site for oxygen.[38] When $O_2$ is bound within hemoglobin, the porphyrin ring is planar, with iron directly in the center and the protein is in the relaxed state (R-state). Deoxyhemoglobin is considered a tense state (T-state) because the porphyrin ring is bent, and iron is 0.4-0.6 angstroms out of the center.[39] Deoxyhemoglobin also has a lower affinity for oxygen binding, as binding is cooperative.

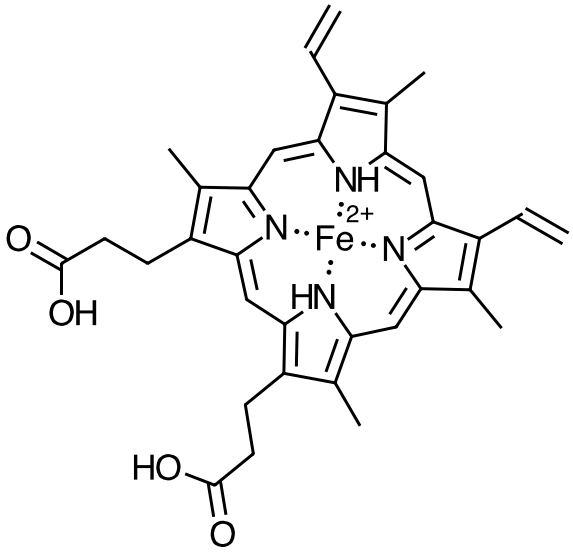


**Figure 1.2** The 2-D structure of heme featuring an iron ion coordinated in the center of a porphyrin ring.[39]

RBCs are typically about 7-8 μm in diameter and have a biconcave shape. Their membrane is extremely flexible which make them capable of fitting through small

capillaries. Comprised of carbohydrates, lipids, proteins and a large amount of salicylic acid, RBC membranes are negatively charged (-15.7mV). [38, 39] RBCs are different from other cells because they do not contain a nucleus as it is unnecessary for their function and aids in their flexibility. It is generally agreed upon that RBCs are not capable of endocytosis which is the active transport of large molecules into the cell. In endocytosis, the membrane engulfs the molecule, ions or solid particle to form an intracellular membrane coated vesicle. The vesicle is eventually broken down to release the contents within the cell. Since RBCs cannot bring extracellular material in through this method, ions and molecules must enter via passive or facilitated diffusion. Diffusion of nonpolar and noncharged species across the cell membrane happens spontaneously due to a difference in concentration in the extracellular and intracellular matrices. Facilitated diffusion brings polar molecules and charged ions into the cell with the use of selective ion channels or carrier proteins.

### 1.5 Previous Studies on Red Blood Cells

One study on fish red blood cells found that AgNPs 15 nm in diameter at concentrations of 10 µg/mL or higher had the greatest effect on the cells in terms of hemolysis, ROS production and membrane injury.[40] The RBCs were washed three times with phosphate buffered saline (PBS), diluted and incubated with various sizes of AgNPs (15, 50 and 100nm) for two hours with concentrations ranging from 1.25 to 20 µg/mL. Following incubation, the RBCs were isolated and washed twice with PBS before analysis. Significant hemolysis was observed when the RBCs were incubated with small AgNPs (15 nm) at concentrations as low as 5 µg/mL. As the concentration was increased to 10 and 20 µg/mL, the percent hemolysis also increased to ~37% and ~64%

respectively. Dark field images showed that AgNPs from 15 to 100 nm were able to enter the cell, and significant aggregation of the NPs >50nm occurred within the cell. An assay measuring superoxide dismutase (SOD) was used to indicate the presence of ROS. The RBCs incubated with the 15 nm AgNPs ≥ 5 μg/mL exhibited the highest concentrations of SOD. The membrane injury, measured with a flow cytometric assay, was most severe with small AgNPs of 15 nm. Concentrations as low as 0.75 μg/mL induced obvious membrane damage. Fish RBCs, contrary to human RBCs, have a nucleus which makes them larger in size.

A few studies have investigated the molecular interaction of AgNPs with RBCs via Raman spectroscopy. In one study, large nanoparticles of 100 nm were incubated with RBCs for 45 hours.[41] Differences in the Raman spectra from the control to the treated cells showed that a conformational change from the R- to T-state had taken place in the hemoglobin. The NPs were too large to diffuse into the cell and affect the hemoglobin directly, which meant the interaction with the membrane induced the change in the hemoglobin.

Another study examined the SERS spectra of RBCs incubated with citrate capped AgNPs for 15 minutes and 18 hours.[42] After 15 minutes, the SERS spectra showed many peaks characteristic of hemoglobin. This indicates only a short period of time is required for AgNP interaction with the band 3 transmembrane protein which binds intracellular hemoglobin. The AgNPs were too large to enter the cell through the protein but the extracellular adhesion to the protein put the AgNPs in close enough proximity to the intracellular bound hemoglobin to enhance the characteristic peaks. The with membrane

bound hemoglobin. Following an 18-hour incubation, Raman shifts corresponding to proteins and lipids suggested alteration or damage of the cell membrane had taken place.

Though these studies showed many interesting results, the uptake and interactions of small AgNPs in human red blood cells was not established.

### 1.6 Knowledge Gaps

The primary motivation of this research stems from the lack of well-established analytical based methods for studying uptake, distribution, aggregation state and molecular interaction of AgNPs in human red blood cells. While many studies have shown the toxicity of the silver nanoparticles both *in vitro* and *in vivo*, much less is known about the uptake and mechanism of interaction between nanoparticles and human red blood cells.

### 1.7 Main Goal and Specific Aims

## Main Goal

The primary goal of this study is to adapt a suite of analytical based methods for characterizing uptake, distribution, aggregation state and molecular interaction of AgNPs in human red blood cells.

## Specific Aims

1. To synthesize, filter and characterize citrate capped AgNPs with tangential flow filtration (TFF), UV-visible spectroscopy, transmission electron microscopy (TEM), inductively coupled plasma optical emission spectroscopy (ICP-OES) and Raman spectroscopy.

2. To quantify the total silver uptake by RBCs using graphite furnace atomic absorption spectroscopy (GFAAS).

3. To determine the distribution, aggregation state and molecular interaction of AgNPs with RBCs using Raman spectroscopy and Cytoviva Hyperspectral imaging.

These aims will be accomplished by synthesizing AgNPs using a modified Lee Meisel synthesis that yields small nanoparticles with an average diameter between 5 and 10 nm. TFF will produce a more monodisperse, concentrated and pure colloid. Packed RBCs (PRBCs) will be washed with PBS to restore membrane shape and function. The washed RBCs will be suspended in a 5% glucose solution and treated with 15 µg/mL of filtered AgNPs at 37ºC for 1 hour. The unbound AgNPs will be removed by washing the unlysed RBCs with a glucose solution prior to resuspension and analysis on GFAAS, Raman, and Cytoviva hyperspectral microscopy. The knowledge obtained from this *in vitro* research will provide useful information about the interaction of AgNPs with human cells. Inferences can be made about the implications of these interactions *in vivo* and the dangers of the growing use of AgNPs within biomedical applications.

## 2. MATERIALS AND METHODS

All solutions used to synthesize AgNPs were purchased as high-grade reagents from Fisher Scientific. Phosphate buffered saline (PBS), 10x solution with a pH of 7.4±0.1 was purchased from Fischer Bioreagents. This PBS was diluted to a 1x solution and stored at 4°C. High quality water with a resistivity of 18MΩ was used for the entirety of the experiment.

### 2.1 Synthesis of Citrate Coated Silver Nanoparticles

A modified Lee-Meisel synthesis was used in this experiment to generate small, spherical citrate capped AgNPs.[43] First, 1.7 mL of a 1% silver nitrate solution was added to 100 mL of water and heated to 90ºC with vigorous stirring. After 15 minutes, 2 mL of a 1% trisodium citrate solution were added, and the reaction vessel was heated and stirred for 1 hour.

## 2.2 Size Isolation and Concentration of Nanoparticles with Tangential Flow Filtration

A tangential flow filtration (TFF) system (Spectrum Labs, Inc.) was used to achieve a pure, more monodisperse, and concentrated colloid (Schematic 2.1). A KrosFlo Research iii system equipped with modified polyether ether sulfone (mPES) Midi Kros filter modules was utilized. The colloid was filtered through a 500 kD (790 $cm^2$, ~ 50 nm pore size) membrane filter to remove large nanoparticles. The permeate was then filtered through a 10 kD (790 $cm^2$, ~ 5 nm pore size) membrane filter to remove smaller nanoparticles, excess reagents and water. The concentrated 10 kD retentate was then characterized and used for incubation with RBCs.

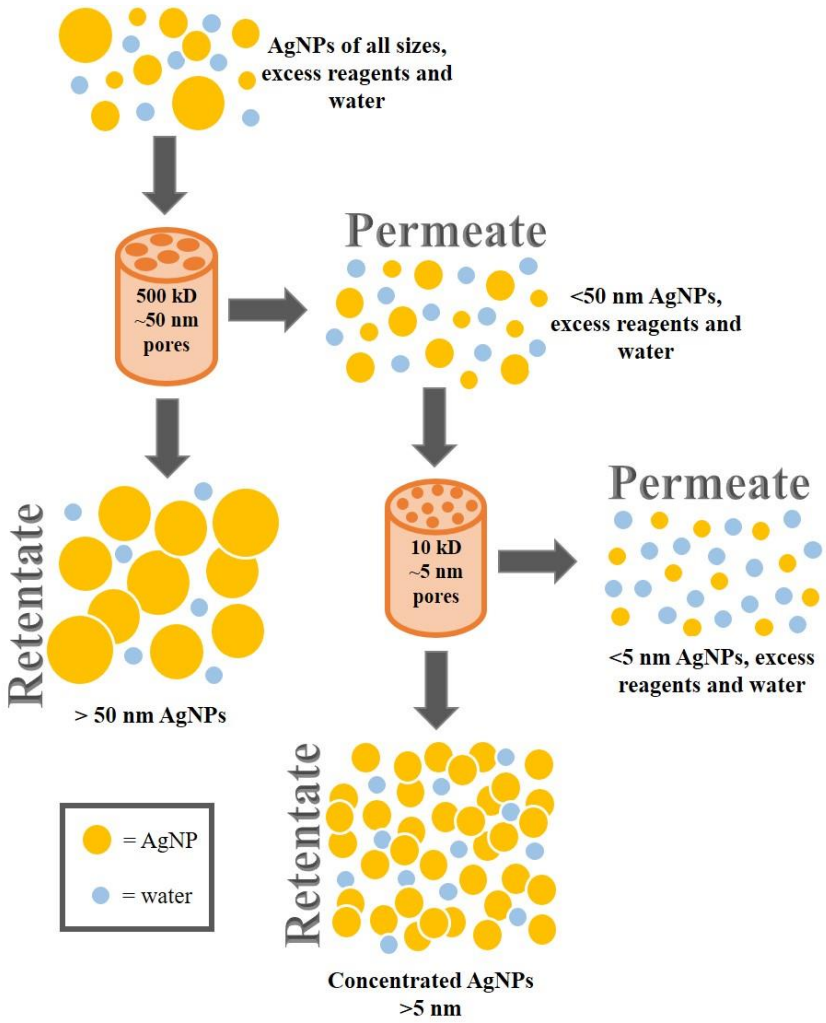


**Schematic 2.1** TFF system used to separate nanoparticles by size and the major species present in the permeate and retentate of each step.

## 2.3 Characterization of Silver Nanoparticles

*UV-Vis absorption spectroscopy* (Cary Bio 50, Varian Inc.): Extinction spectra of synthesized and filtered AgNPs were collected at a scan rate of 1200 nm $min^{-1}$ in a 1 cm, quartz cuvette and baseline corrected with water or glucose depending on which solution the NPs were dispersed.

*Raman spectroscopy* (LabRam HR-800, Horiba Jobin Yvon, Inc.): Raman spectra of synthesized AgNPs (100-2000 $cm^{-1}$) were collected in quartz cuvettes. The acquisition setup consisted of a confocal Raman BX41 microscope, an internal helium neon laser of 632.8 nm (15 mW output), Olympus 100x and 50x objectives, a holographic grating of 600 grooves $mm^{-1}$, a confocal hole of 300 µm, and a thermoelectrically cooled Andor CCD camera of 1024 x 256 pixels. Three cycles with 30 second exposures were collected and averaged using the LabSpec v.5 software. The spectral resolution was ~ 1 $cm^{-1}$.

*Inductively coupled plasma optical emission spectroscopy* (ICP-OES, Varian 710-ES): AgNP samples were digested using trace metal grade nitric acid (Fisher Scientific) in glass beakers, the volume of the digested sample was reduced with heat. The liquid was allowed to cool, quantitatively transferred and diluted with high quality water to obtain a 2% nitric acid matrix. Silver standards (0-500 µg $L^{-1}$) were prepared from the stock Ag standard (1,000 mg $L^{-1}$) (CentraPrep) by quantitative dilution in 2% nitric acid. Samples were supplied into the ICP-OES instrument with an autosampler (Varian SPS 3) at a peristaltic pump rate of 2 mL $min^{-1}$, nebulized and further pumped into the axially positioned quartz torch. Triplicate measurements were obtained at the two main emission lines of Ag (323.068 nm and 338.289 nm). The operating conditions were as follows: nebulizer pressure of 200 kPa, plasma flow of 15.0 L $min^{-1}$, auxiliary flow of 1.50 L $min^{-1}$, radio-frequency power of 1.20 kW, replicate read time of 15 s, internal stabilization delay of 45 s, sample uptake delay of 40 s and rinse time of 15 s. The LOD and LOQ are 3 ppb and 5 ppb respectively.

## 2.4 Treatment and Incubation of Red Blood Cells

*Pre-treatment of Packed RBCs:* PRBCs were received from the Community Blood Center of Dayton, Ohio. The blood was donated from a healthy adult with a blood type AB+. The blood bank separated the RBCs, screened them for HBV (Hepatitis B Virus), HCV (Hepatitis C Virus), HIV-1, HIV-2 (the human immunodeficiency virus that causes AIDS), HTLV (Human T-cell Lymphotropic Virus), syphilis, West Nile Virus (WNV), Chagas Disease, ZIKA Virus to ensure that the blood is healthy. The RBCs were then stored with anticoagulant and preservation solutions and stored at 4°C prior to analysis. To remove the preservation and anticoagulant solutions, citrate phosphate dextrose solution (CPD) and AS-5 (Optisol) respectively, a 2 mL aliquot of PRBCs were centrifuged at 10,000 rpm for 10 minutes. The separated RBCs were washed three times with 1 mL phosphate buffered saline (PBS) and spun at 10,000 rpm for 10 minutes, removing the supernatant between washes. The PBS was kept at 4°C to keep the RBCs cool during the washing process.

*Incubation and Post-treatment of Red Blood Cells:* Washed RBCs were added to a solution containing 5% glucose and filtered AgNPs to achieve a total silver concentration of 15 μg $mL^{-1}$, an osmolality of 0.20 and hematocrit of 32±3%. The suspended RBCs were incubated at 37°C for one hour, with gentle agitation every 15 minutes. Following incubation, the RBCs were separated and washed an additional 3 times with 5% glucose via centrifugation at 3000 rpm for 10 minutes to remove unbound AgNPs. To ensure reproducible results, triplicate incubations were performed and analyzed. A control was performed in which RBCs were incubated solely with 5% glucose (vehicle) following

identical treatment as mentioned prior. The rest of the procedure was carried out in the same manner as the AgNP exposed cells.

RBCs were counted prior to incubation and following the third post-wash with a (Hausser Scientific) hemocytometer. To determine the hemolysis that occurred during the incubation and post-wash process, the hematocrit of incubation solution was compared to the AgNP exposed cell solution. Capillaries filled with the solutions, sealed with Hemato-seal (Fisherbrand) and centrifuged at 10,000G for 5 minutes. The percentage of RBCs in solution was determined by height.

## 2.5 Preparation and Analysis of Red Blood Cells

*Graphite Furnace Atomic Absorption Spectroscopy* (GFAAS, Varian 240-FS, GTA 120): RBC samples were digested in trace metal grade nitric acid (Fisher Scientific), bleached with 2 mL of 30% hydrogen peroxide (Fisher Scientific) and the volume of the digested samples was reduced with heat. The digested samples were quantitatively transferred and diluted with high quality water to obtain a 2% nitric acid matrix. The autosampler made and analyzed 10 calibration standards from a 10 ng $mL^{-1}$ Ag in 2% nitric acid stock solution. The autosampler supplied 10 µL aliquots into the graphite tube in triplicate measurements for analysis. The instrument parameters for the drying, charring and atomization processes can be seen in Table 2.1 below. A silver hollow-cathode lamp was used at an excitation wavelength of 328.1 nm with a slit width of 0.5 nm and an operating current of 40 mA. The flow rate for the argon purge gas was set to 0.3 L $min^{-1}$.

**Table 2.1.** GFAAS instrument parameters.

| **Drying** | |
|---|---|
| Temperature | 120ºC |
| Time | 10 s |
| **Charring** | |
| Temperature | 400ºC |
| Time | 8 s |
| **Atomization** | |
| Temperature | 2000ºC |
| Time | 5 s |

*CytoViva Hyperspectral imaging*: RBCs were suspended in a 5% glucose solution, smeared on a glass slide and sealed with vaseline. The CytoViva hyperspectral imaging system (Auburn, AL) is comprised of an Olympus research grade optical microscope, enhanced darkfield optics, full spectrum aluminum halogen source illumination, a Z stepper motor and integrated hyperspectral imaging capabilities. Real-time images of AgNP exposed RBCs were collected along with hyperspectral maps corresponding to dark-field scattering spectra in the 400-1000 nm region with 2 nm spectral resolution hyperspectral imaging system. The Z stepper motor allowed high-resolution 3D images of the cells to be captured. Images were collected every 100 nm and interpolated in ImageJ to create 3D images of an AgNP exposed RBC. Hyperspectral images were compared to spectra of vehicle control (glucose incubated) RBCs and filtered AgNPs in 5% glucose. Hyperspectral data analysis was performed on a custom version of ENVI 23 hyperspectral image analysis software.

*Raman spectroscopy* (LabRam HR-800, Horiba Jobin Yvon, Inc.): RBCs were suspended in a 5% glucose solution and placed on a glass slide. The laser was focused within the solution and on individual cells. The analysis parameters were the same as previously

stated (Section 2.3) except the acquisition time was set to 10 s to avoid photodamage of the RBCs.

# 3. RESULTS AND DISCUSSION

## 3.1 Characterization of Synthesized Nanoparticles

The synthesized citrate colloid was filtered using TFF to achieve a more monodisperse and concentrated colloid. The filtered colloid was characterized with UV-VIS, Raman and ICP-OES to determine the size, purity and concentration. Figure 3.1 shows the surface plasmon resonance peak at 390 nm, which is characteristic of citrate capped silver nanoparticles with an average diameter of 5-10 nm. The peak of the filtered colloid is slightly narrower which confirms that the filtered colloid has less variation in the average diameter. Isotonic PBS is typically used for incubations with RBCs, however, addition of filtered AgNPs to PBS immediately induced aggregation. The aggregated AgNPs showed no characteristic plasmon peak. The aggregation can be attributed to the interaction of positive ions like calcium and potassium in the saline with the negatively charged citrate coating. A previous study showed the same results in PBS but proved aggregation did not occur when citrate capped AgNPs were dispersed in a 5% glucose solution.[44] Glucose, often referred to as blood sugar, is readily taken into RBCs via the Glut1 transmembrane protein. With the same tonicity and osmolarity as PBS and plasma, a 5% glucose solution was a logical replacement for PBS in the incubation and post-washing process. When the filtered colloid was dispersed in a 5% glucose solution, no aggregation occurred as illustrated in Figure 3.1.

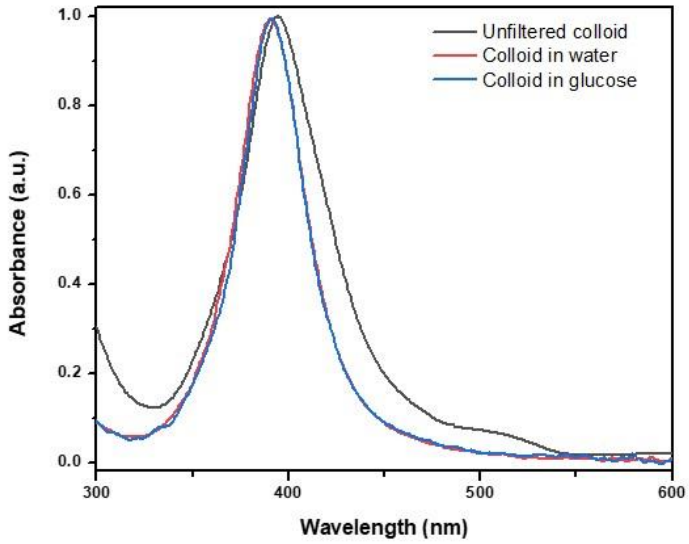


**Figure 3.1** Surface plasmon resonance peak of the unfiltered colloid suspended in water, the filtered colloid suspended in water and in 5% glucose solution.

Table 3.1 shows the wavelength maxima and full width at half maximum (FWHM) values which give information about the average diameter and size distribution of the colloids. The higher the wavelength maxima, the larger the average diameter. Broader peaks indicate a larger size distribution of NPs is present in the colloid.[21] The FWHM values were calculated using the gaussian fit on Origin. The filtered colloids have a slightly lower maximum wavelength than the unfiltered which indicates that the average size is smaller in diameter. The FWHM is significantly larger for the unfiltered colloid, further supporting the size selectivity principle of TFF. The wavelength maximum and FWHM value did not increase when the filtered colloid was suspended in a glucose solution proving aggregation did not occur.

**Table 3.1** Surface plasmon resonance maxima and FWHM values for the unfiltered colloid suspended in water, filtered colloid suspended in water and in 5% glucose solution.

| Colloid Sample | Maximum Wavelength (nm) | FWHM (nm) |
|---|---|---|
| Unfiltered in water | 394 | 59.4 |
| Filtered in water | 390 | 44.8 |
| Filtered in glucose | 391 | 43.3 |

The concentration of silver was monitored throughout the filtration process to ensure that the TFF was working properly and to draw conclusions about the sizes of NPs produced in this modified Lee-Meisel synthesis. These concentrations, along with the final concentration of the filtered colloid were obtained via ICP-OES. Figure 3.2 shows a representative calibration curve of various standards in 2% nitric acid. The limit of detection (LOD) and limit of quantification (LOQ) were both 5 ng $mL^{-1}$ and of the colloid concentrations had a low percent RSD of <3%.

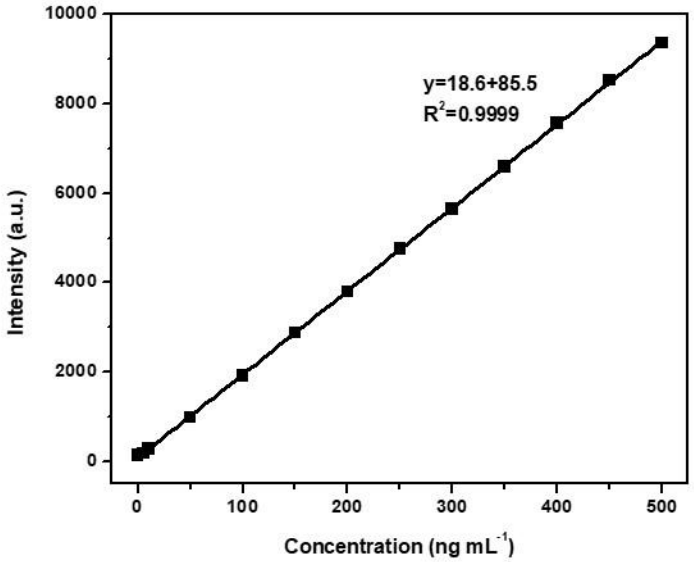


**Figure 3.2** A representative ICP-OES calibration curve used to determine silver concentration in filtered colloid samples.

Table 3.2 below summarizes the ICP-OES results and confirms that the TFF was functioning correctly. The modified Lee-Meisel synthesis used in this experiment produced a significant number of large NPs (> 50 nm) that were removed with the 500 kD filter. This step alone increased the concentration of the colloid by almost 2-fold. The 10 kD filter removed a very small amount of silver which was below the LOQ. This means there was very little excess silver ions from the synthesis and small NPs in the original colloid. This step also concentrated the colloid significantly, bringing the final concentration of filtered colloid to 550 µg $mL^{-1}$ when 1 liter of the original colloid was filtered. When larger volumes of the original colloid were concentrated with the 10 kD filter, concentrations as high as 3,500 µg $mL^{-1}$ could be achieved. Colloids with such high concentrations were only stable for two weeks when stored at 4°C.

**Table 3.2** Concentration of silver in each filtered colloid sample determined via ICP-OES.

| Colloid Sample | Size Range | Concentration (µg $mL^{-1}$) |
|---|---|---|
| Original Colloid | All sizes | 115 |
| 500 kD Permeate | < 50 nm | 206 |
| 500 kD Retentate | > 50 nm | 256 |
| 10 kD Permeate | < 5 nm | < 5 |
| 10 kD Retentate | 5-50 nm | 550 |

Figure 3.3a shows the Raman spectrum of the filtered colloid showed only water peaks (1648, 3232 and 3398 $cm^{-1}$) indicating that the excess reagents were filtered out with the 10 kD filter and the colloid is pure.[45] To test the SERS capability of the filtered AgNPs, the aggregated colloid was added to a $10^{-6}$ M solution of rhodamine 6G (R6G), a common Raman signaling agent.[46] The signal of the R6G Raman shifts increased by 15,000 counts

due to the formation of hotspots between the citrate capped AgNPs illustrating the potential of SERS enhancement in RBCs (Figure 3.3b).

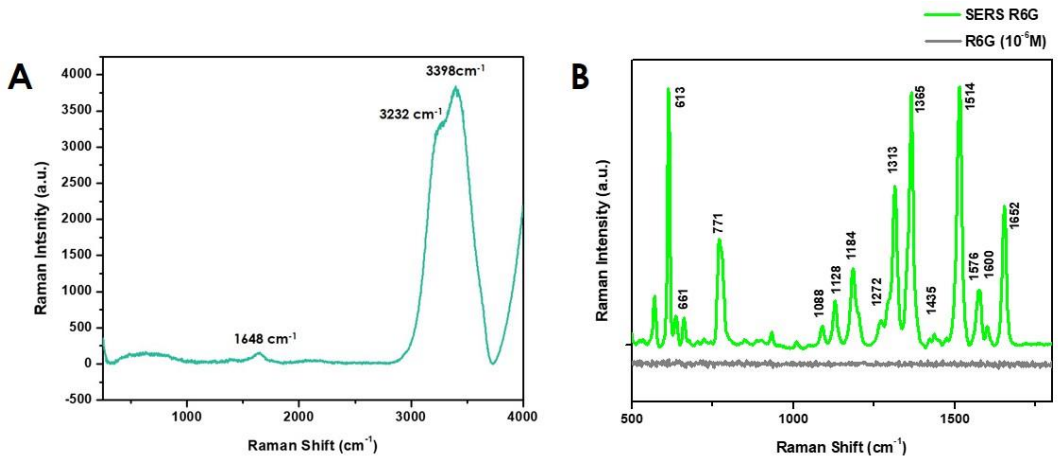


**Figure 3.3** A) Raman spectrum of the filtered colloid. B) Background corrected Raman spectra of a solution of R6G and SERS enhancement of R6G when the filtered colloid was added.

TFF size selected, concentrated and purified the synthesized colloid which resulted in a 550 µg $mL^{-1}$ colloid of citrate capped AgNPs that were approximately 5-10 nm in diameter and exhibited promising SERS capability.

## 3.2 Treatment and Incubation of Red Blood Cells

*Treatment of Packed Red Blood Cells:* The packed RBCs were stored in an anticoagulant and preservation solution. The cells were washed thrice with PBS to remove these solutions, restore the membrane shape and remove cellular debris. UV-VIS was utilized to monitor the amount of hemoglobin in the supernatants throughout the washing process. Hemoglobin absorbs at 5 distinct wavelengths which is consistent with literature.[47, 48, 49]

Three of which are assigned and well used in hemoglobin measurements, the Soret at 417 nm and the Q bands at 542 and 578 nm.[50] Since the Soret band is the most intense, it was used for all quantifications in this experiment.

To determine the number of pre-washes (pre-incubation washes) that were appropriate, 5 washes were performed and the hemoglobin in the supernatants was monitored. Figure 3.4 shows the normalized absorbance spectra of the supernatants for the washes with PBS. The hemoglobin absorbances decrease in the first four washes which indicates the removal of cellular debris resulting from cells that lysed due to storage. There was a slight increase in the absorbance of the last wash. This means that during the fifth wash, more RBCs lysed and released hemoglobin into the supernatant meaning 5 pre-washes was too much mechanical manipulation for the RBCs to sustain.

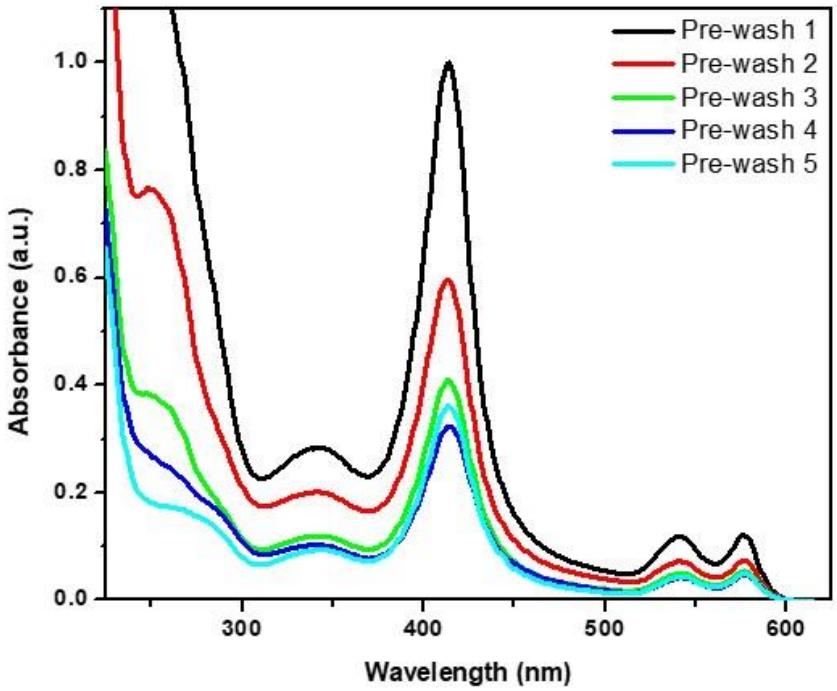


**Figure 3.4** UV-VIS spectra monitoring the characteristic hemoglobin peaks in pre-wash supernatants.

A paired t-test was performed on the absorbance maxima of the Soret band and the results are recorded below (Table 3.3). The decrease in absorbance between washes one and two was the only significant difference at a 95% confidence interval (CI). Even though the release of hemoglobin into the supernatant during wash three was not significant, three pre-washes were performed for the remaining experiments to conform with previous studies and ensure restoration of membrane function and shape.

**Table 3.3** Statistical analysis of the Soret (417 nm) peak in the pre-wash supernatants (N=4).

| Washes | 95% CI t critical | Experimental t value | Significance |
|---|---|---|---|
| **1-2** | 3.18 | 3.48 | Significant |
| **2-3** | | 2.22 | Insignificant |
| **3-4** | | 1.33 | Insignificant |
| **4-5** | | -1.52 | Insignificant |

The pre-washed blood was counted with a hemocytometer and was found to have $5.9x10^6$ cells $\mu L^{-1}$ which is within the normal range for men and slightly higher than the normal range for women.[51] Thus, it is suspected that the RBCs used in this experiment were donated from a male but there are no confirmatory tests that could be performed. The washed RBCs were then incubated in a 5% glucose solution with the filtered AgNPs.

*Incubation and Post Treatment of Red Blood Cells:*

Three trials were performed treating the RBCs with the filtered AgNPs along with a vehicle control group where RBCs were treated solely with a 5% glucose solution. The ratio of 5% glucose solution to RBCs was optimized to be close to that of plasma to RBCs in the body. The hematocrit of incubation solution was determined to be 32±3% which is slightly lower than average range for both men and women.[52] The hematocrit couldn't be increased further without compromising the accuracy of the volume of RBCs in the incubation solution. Increasing the volume ratio of RBCs to glucose solution made it impossible to accurately transfer the RBCs via pipetting.

The unbound AgNPs were removed prior to ICP-OES, Raman and CytoViva analysis via post-(incubation) washes with a 5% glucose solution. The incubation solution and post-wash supernatants were also monitored on UV-VIS. The concentration of hemoglobin in

the supernatant decreased with each subsequent wash meaning the cellular debris from the hemolysis that occurred during the incubation process was removed (Figure 3.5).

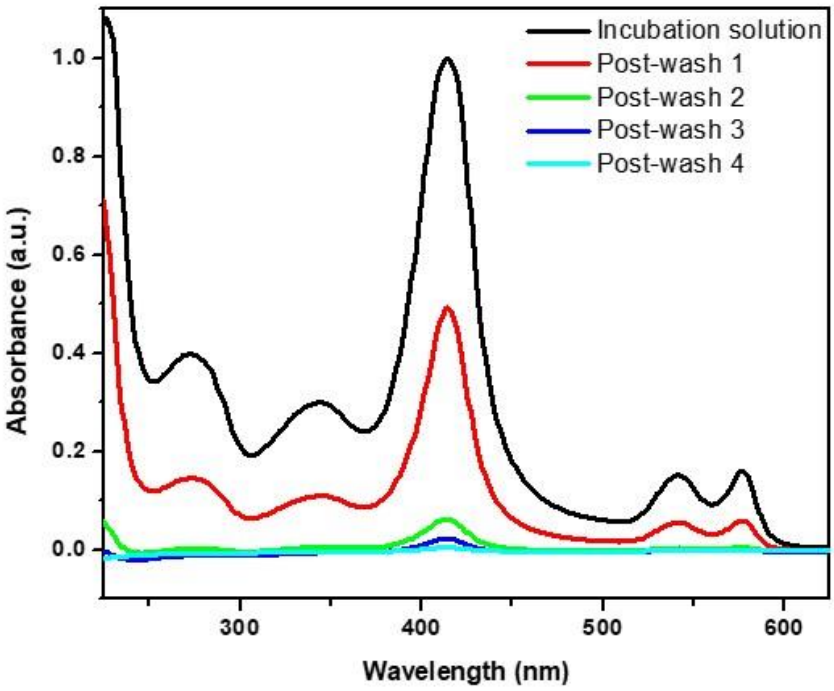


**Figure 3.5** UV-VIS spectra monitoring the characteristic hemoglobin peaks in the incubation solution and post-wash supernatants.

Since the surface plasmon peak for the colloid is very close to the Soret absorbance (391 nm and 417 nm respectively), the FWHM values were determined using the gaussian fit on Origin. The FWHM values of this peak did not significantly increase from those seen in the pre-washes indicating there was not enough AgNPs present in the supernatants to alter the width. The Soret band was again analyzed to determine the number of post-washes necessary before analysis (Table 3.4). The first two post-washes decreased the concentration of hemoglobin significantly, but the third and fourth wash yielded an

insignificant decrease. Three post-washes were performed for the remainder of the experiment to make certain the majority of the unbound AgNPs were removed before quantification via ICP-OES.

**Table 3.4** Statistical analysis of the Soret (417 nm) peak in the post-wash supernatants (N=4).

| Washes | 95% CI t critical | Experimental t value | Significance |
|---|---|---|---|
| **0-1** | 3.18 | 13.4 | Significant |
| **1-2** | | 14.6 | Significant |
| **2-3** | | 2.85 | Insignificant |
| **3-4** | | 2.87 | Insignificant |

UV-VIS is a commonly used technique to characterize silver nanoparticles, but it also proved to be useful in the method development for the treatment of RBCs.

## 3.3 Quantification of the Uptake of Silver Nanoparticles into Red Blood Cells

Though AgNPs that are capped with biocompatible species (like citrate) are not dangerous themselves, over time they will release silver ions which have proven to have adverse and toxic effects in many cell lines.[27, 29] For this reason, it is extremely important that the uptake of silver nanoparticles in human cells is well known. To quantify the amount of silver that adhered to and entered the cells during incubation, AgNP exposed cells were counted, digested in acid and analyzed via GFAAS. A calibration curve is shown below (Figure 3.6). The LOQ was 0.5 ng $mL^{-1}$ and a calibration check was performed every three samples to ensure accuracy.

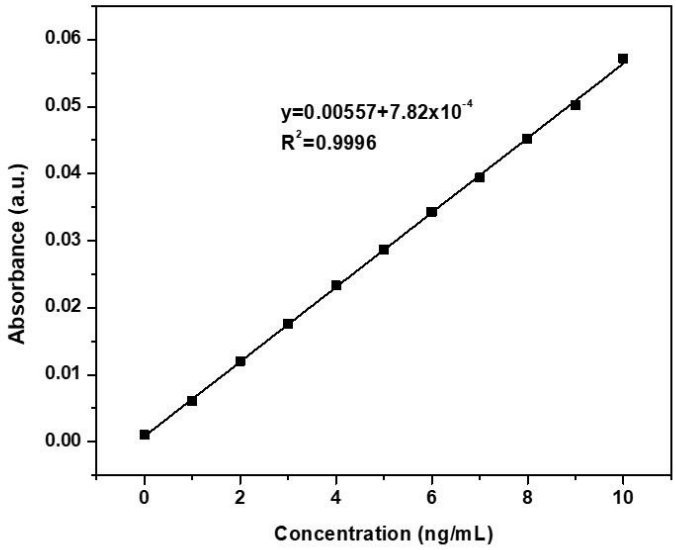


**Figure 3.6** Representative graphite furnace calibration curve of silver used to quantify silver in AgNP exposed RBC samples and supernatants.

Table 3.5 shows the quantity of silver in the incubation solution and the amount of silver that was taken up by the cells from three different incubation trials from one unit of RBCs (one donor). The µg of silver in the incubation solution was assumed to be the total silver, or 100%. That total was used to calculate the percentage present in the incubation supernatant, post-wash supernatants and AgNP exposed RBCs. The incubation supernatant was the original separation of glucose solution and lysed RBCs from the unlysed AgNP exposed cells via centrifugation before fresh glucose solution was added in the first prewash.

**Table 3.5** Amounts and percentages of silver in the incubation solutions, post-wash supernatants and AgNP exposed RBCs determined via GFAAS. Three separate incubation trials were performed using the same unit of RBCs.

| | **µg of Silver** | | | **Percentage** |
|---|---|---|---|---|
| | Trial 1 | Trial 2 | Trial 3 | |
| Incubation solution | 33.35 | 33.56 | 35.11 | 100 ± 0 |
| Incubation supernatant | 17.82 | 18.32 | 12.89 | 48 ± 10 |
| Post-wash 1 supernatant | 0.90 | 1.49 | 4.55 | 7 ± 6 |
| Post-wash 2 supernatant | 0.08 | 0.07 | 0.23 | 0.4 ± 0.3 |
| Post-wash 3 supernatant | 0.03 | 0.04 | 0.04 | 0.11 ± 0.01 |
| AgNP exposed RBCs | 14.15 | 16.95 | 17.61 | 48 ± 5 |

The first two trials showed very similar results in that the majority (54%) of the unbound AgNPs were removed in the first separation (incubation supernatant) prior to a glucose wash. The amount of silver removed from each subsequent wash decreased to 0.1% in the last post wash. During the third trial, only 37% of the unbound NPs were removed prior to the first wash. The majority of the remaining unbound AgNPs were removed (13%) in the first wash. By the 3rd wash there was still an extremely small percentage of less than 0.15% that was removed. This small percentage could be attributed to intracellular AgNPs that were released from cells that lysed during centrifugation. These percentages, along with the UV-VIS data proves the 3 post-washes with glucose are sufficient to remove almost all the lysed cells and the unbound NPs. Even though there were inconsistencies in the removal of unbound AgNPs, the amount of silver in the post-washed AgNP exposed cells were fairly consistent with an average of 48±5%. This is a high percentage in comparison to most studies that have been done with other human cells. Studies of AgNPs in kidney and liver cancer cells showed less than 15% uptake.[27, 53, 54] One study with 10 nm AuNPs showed a fairly high percent uptake (36%) in human

epithelial cells.[56] Interestingly, no significant difference in the percent uptake was observed when comparing citrate capped NPs versus noncapped NPs. Larger AuNPs of 25 nm were not taken up as readily, proving that size plays a role in uptake mechanisms.[56] Another study proved the effects of nanoparticle size on uptake. Citrate capped AgNPs exposed to pulmonary epithelial cells exhibited percent uptake ranging from 50-65% depending on the size.[57] In this study, significant uptake of the highly negative AgNPs was observed even though the cell membrane has a negative charge overall. Though cell membranes are negative, small areas exist that are positively charged, and these areas are responsible for the strong interactions taking place with the AgNPs.[58] When the same AgNPs were exposed to a different cell line, the uptake dropped significantly due to the difference in the makeup of the cell membrane. These studies on epithelial cells showed that the percent uptake is largely dependent on the size of the nanoparticles and the specific cell line.

The results of these studies suggest that the small size of the nanoparticles in combination with the negative citrate coating, was the main cause for the high percent uptake of the AgNPs in RBCs. It is also clear the cell type can greatly affect the uptake so the makeup of the membrane of RBCs must be another contributing factor. Though epithelial cells are different from RBCs in that they can undergo endocytosis, smaller NPs are still more likely to enter RBCs because ion channels and other transmembrane proteins have small diameters. RBCs are also negatively charged overall, but the outer layer of the membrane contains phospholipids which have positively charged amine groups. There are also membrane proteins which can be positively charged due to the presence of three basic amino acids (Lys, His, Arg). To my knowledge, no other studies have quantified the

uptake of AgNPs in RBCs. Further studies should be done to quantify the uptake of AgNPs of various sizes and surface coatings in RBCs to further confirm these suppositions.

A significant number of cells lysed during the incubation and post-washing process due to the use of 5% glucose as the vehicle solution. Hematocrit measurements were averaged from three trials of both vehicle control cell suspensions (incubated solely with glucose) and AgNP exposed cell suspensions. In both the control cells and AgNP exposed cells, the hematocrit dropped from 32±3% prior to incubation, to 12±1% in the post-washed cell suspensions proving that the AgNPs did not impact the hemolysis. These measurements showed that 62±4% of the cells lysed, however, they were taken independently and approximately a week after the three trials used for the GFAAS analysis. Cell counts were taken of the GFAAS trials used to quantify the silver up taken by the RBCs. These counts revealed that 81±7% of the cells lysed in the three GFAAS trials. This hemolysis is higher than what has been seen previous studies, so a control was performed in which the cells were pre-washed, incubated and post-washed with PBS (in the absence of AgNPs). In this control, both hematocrit measurements and cell counts showed that significantly less hemolysis occurred (8% and 7% respectively). This proves that the 5% glucose solution caused the hemolysis observed in the experiment. Although a 5% glucose solution is isotonic to plasma, glucose is readily taken into the cell. As the glucose concentration in the vehicle solution decreased, the solution became hypotonic which caused the cells to lyse. The small percentage of cells that did not lyse were likely smaller in size (more shrunken) prior to incubation. Thus, when the vehicle solution became hypotonic, the cells expanded to a normal size. This also explains the

discrepancy between the percent hemolysis determined via counting and hematocrit measurements when the 5% glucose solution was used. The hematocrit measurements were taken at a later date. The longer PRBCs are stored, they become more shriveled, smaller in size and the membrane loses flexibility. When the hematocrit measurements were taken, the cells were more shrunken so the hypotonicity of the solution restored them to a normal size. Therefore 19% less of the cells hemolyzed than when the experiment was performed a week prior.

Since the cells in the incubation solutions and the AgNP exposed samples of the three trials used to quantify silver on GFAAS, the quantity of Ag per RBC was able to be calculated. The incubation solution averaged to $1.93\pm0.53 \times 10^{-8}$ µg/RBC. Due to the large percentage of cells that lysed and the high percent uptake, the average amount in the post-washed AgNPs exposed cells was significantly higher at $5.57\pm0.86 \times 10^{-8}$ µg/RBC. The large uncertainty in these values is because the third trial was performed a few days later than trials 1 and 2 so the cells were smaller and behaved differently in the presence of AgNPs.

Since the 5% glucose solution caused the cells that were normal or large in diameter prior to incubation to hemolyze, the cells that were analyzed are not a true representation of healthy human RBCs. Future studies should investigate other vehicle control solutions that do not become hypotonic during incubation to determine the true uptake of silver NPs in RBCs that are normal in size.

### 3.4 Determination of the Distribution, Aggregation State and Molecular Interaction of Silver Nanoparticles with Red Blood Cells

After an hour incubation and three post-washes, CytoViva microscopy and Raman spectroscopy, were utilized to examine the distribution and molecular interaction of AgNPs with RBCs. Triplicate incubations were performed to ensure that results were reproducible. Independently, cells were incubated with a 5% glucose solution in which no AgNPs were added as a vehicle control group.

When the filtered colloid was suspended in a 5% glucose solution and imaged on the CytoViva dark-field microscope, various colored nanoparticles were observed (Figure 3.7a). Nearly 1,000 nanoparticles were counted with the particle counter function on ENVI and it was determined that 84% of the nanoparticles appeared blue and had an average hyperspectral maximum of 464 nm (Table 3.6). 13% were green (554 nm) while only 3% were red (637 nm). Since it has been shown that wavelength maxima is directly proportional to the average metallic NP diameter, conclusions could be drawn about the size of the AgNPs using the hyperspectral data collected on the CytoViva. Based on the increases in the hyperspectral maxima, it can be concluded that the blue nanoparticles are the smallest with a diameter of 5-10 nm (as determined via UV-VIS, Figure 3.1). The green NPs are slightly larger in size and the largest NPs appear red.

About 60% of the vehicle control RBCs appeared to be spherocytes meaning the cells were swollen due to the hypotonicity of the incubation solution after the glucose was taken into the cells (Figure 3.7b). The other 40% of cells appeared have a normal doughnut shape and were ~8 μm in diameter. The AgNP exposed RBCs showed interesting results. AgNPs and RBCs were hand counted to quantify the cells that showed interactions and the types of interactions present. About 40% of cells showed no

interaction with the AgNPs, but the other 60% of the cells had blue, green and red extracellular nanoparticles on the cell membrane. The strong adsorption to the membrane is likely a result of the interaction of the negatively charged citrate coating with the positively charged amino groups on sphingomyelin and the quaternary ammonium ion on phosphatidylcholine which are found on the outer most layer of the RBC membrane. The same interaction of citrate capped silver nanoparticles to cell membranes have been seen in previous studies with fish RBCs and membrane models doped with cholesterol.[40, 59] In both experiments, the AgNPs were dispersed in PBS rather than a 5% glucose solution which means the solution did not become hypotonic and cause the cells to swell and lyse. Since the strong membrane interactions were seen in the PBS incubated cells and the 5% glucose incubated cells, it is suspected that the hypotonicity of the 5% glucose solution used in this experiment did not play a role in the strong cell membrane interactions.

The extracellular AgNPs interactions with the membrane did not seem to cause obvious membrane damage because the cells appeared to be spherocytes or donuts (round in shape) and about 8 μm in diameter. However, cells that had significant intracellular interactions showed serious membrane damage. Approximately 30% of NPs entered the cells and can be seen internalized within the cytoplasm. Only the smaller NPs, blue and green in color, were observed within the cells. One explanation for this observation could be due to the fact only a small percentage (3%) of the AgNPs exposed to the cells were red and only about 100 cells were imaged on the CytoViva. Another explanation could be because only passive and facilitated diffusion is possible across the cell membrane. The ion channels and transporter proteins have very small openings, thus only the smaller intracellular AgNPs were observed. The lack of red intracellular AgNPs proves that

aggregation of intracellular AgNPs did not occur. Less than 5% of cells, like the inset in Figure 3.7c, have a significant number of intracellular AgNPs and appear crenated. This would indicate that there was some sort of damage to the membrane which made internalization of the AgNPs easier. Even when numerous NPs were found within the cell, they were blue and green in color which means they were not aggregated.

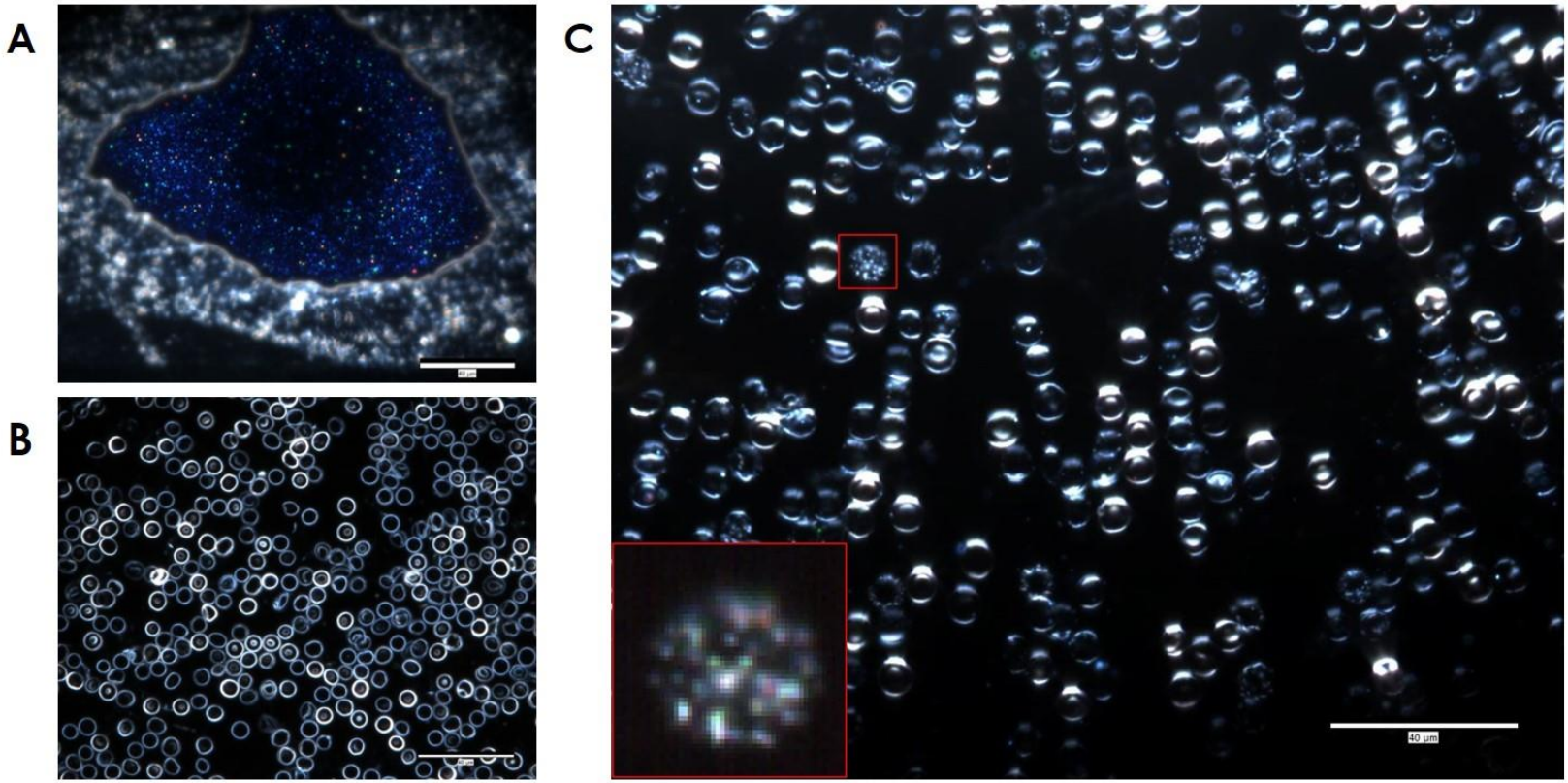


**Figure 3.7** Representative CytoViva images of A) the filtered colloid dispersed in a 5% glucose solution B) the vehicle control RBCs C) the AgNP exposed RBCs. The inset shows a cell with multiple blue and green intracellular and extracellular AgNPs. Scale bars represent 40 µm.

Various images of the AgNP exposed cells were collected and analyzed. The observed AgNPs were determined to be extracellular if there were seen along the membrane, were bright in color and had a high spectral intensity. The intracellular AgNPs could be seen in the middle of cells, had dimmer colors and much lower relative intensities. As can be seen in Figure 3.8, the extracellular AgNPs interaction with the cell membrane caused the dark-field scattering peak to become much broader.[60]

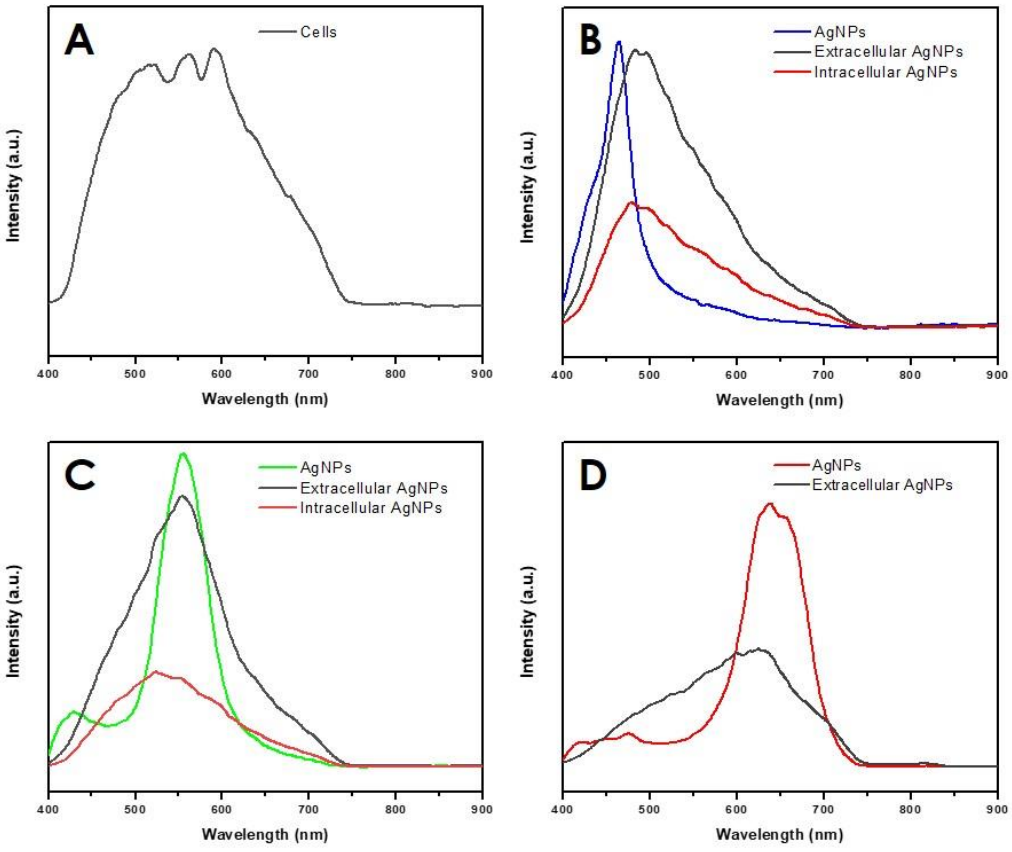


**Figure 3.8** Averaged hyperspectral image of A) the vehicle control RBCs. Averaged hyperspectral image of filtered colloid in a 5% glucose solution (AgNPs), AgNPs adhered to the cell membrane (extracellular AgNPs) and AgNPs within RBCs (intracellular AgNPs) for B) blue nanoparticles C) green nanoparticles and D) red nanoparticles (N=10).

This broadening is also illustrated by the full width at half maximum values which are presented in Table 3.6. The intracellular AgNPs FWHM values are the largest due to the interaction with hemoglobin which has an extremely broad peak ranging from 475 to 750 nm.[60] Cholesterol, phospholipids, spectrin and other components of the cell membrane have fairly broad peaks from 500 to 800 nm.[60] AgNP interaction with these cellular components explains the broadening of the extracellular peaks. The wavelength maximum of the blue extracellular AgNPs shift up from 464 to 490 nm whereas the red extracellular AgNPs max shifts down to 624 from 637 nm. Both are shifts toward 600 nm which is indicative of the interaction with cholesterol and phospholipids which both maximum wavelengths around 600 nm.[60]

**Table 3.6** Peak areas for various Raman shifts observed in the vehicle control, AgNP exposed RBCs and RBC clusters.

| Sample | Maximum Wavelength (nm) | FWHM |
|---|---|---|
| Cell membrane | 514 | - |
| | 561 | - |
| | 590 | - |
| Blue AgNPs | 464 | 60.6 ± 0.5 |
| Blue Extracellular AgNPs | 490 | 142 ± 1 |
| Blue Intracellular AgNPs | 479 | 153 ± 2 |
| Green AgNPs | 554 | 67.3 ± 0.6 |
| Green Extracellular AgNPs | 555 | 144 ± 0.7 |
| Green Intracellular AgNPs | 523 | 159 ± 0.8 |
| Red AgNPs | 637 | 80.0 ± 0.5 |
| Red Extracellular AgNPs | 624 | 192 ± 1 |

Though it was assumed that some AgNPs were internalized within the RBCs due to their spectra and appearance, the presence of intracellular AgNPs was confirmed with the 3D function on CytoViva. Images were collected every 100 nm as the sample was moved in the Z direction toward the objective. Images showing the internalization of AgNPs can be seen in Figure 3.9 below.

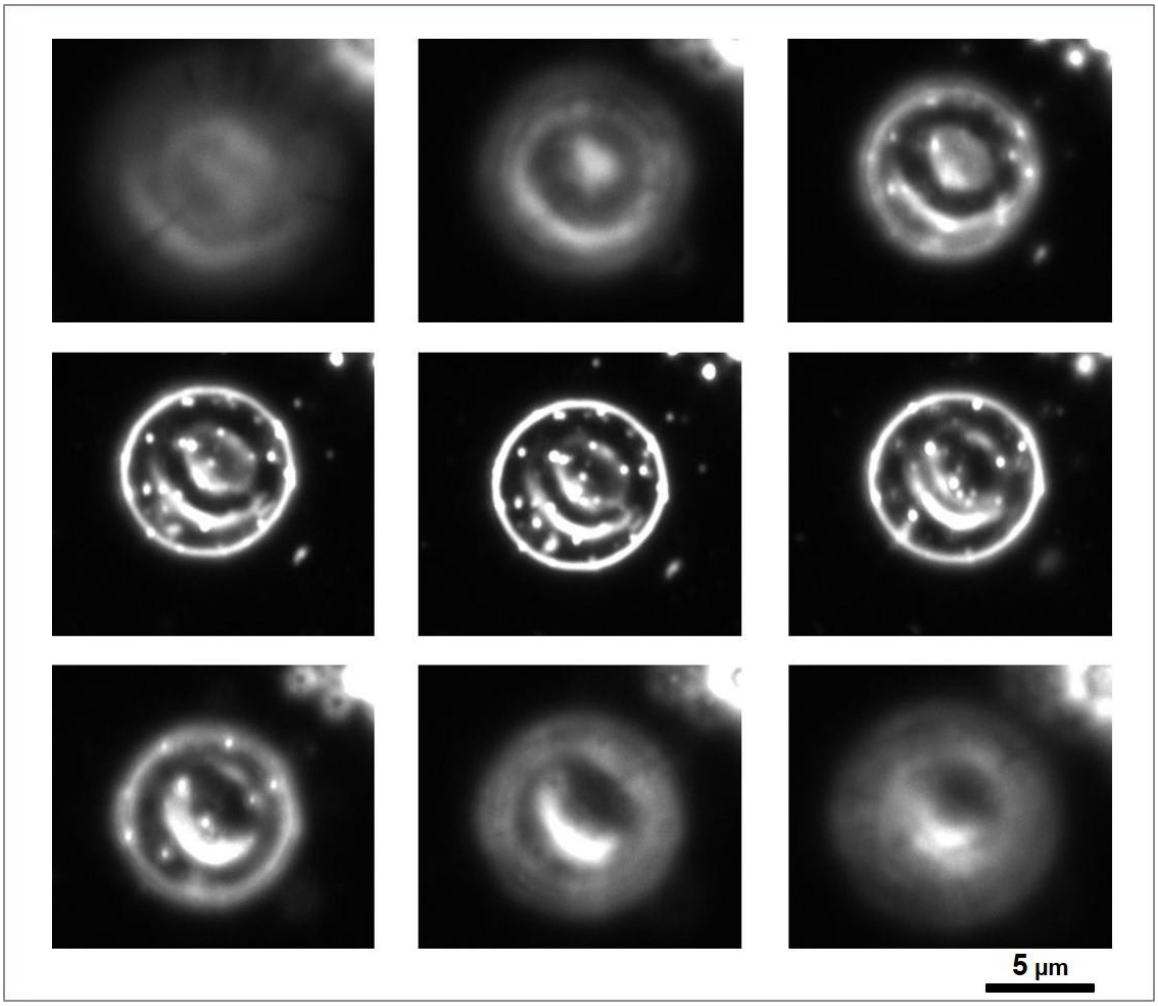


**Figure 3.9** 3D Cytoviva images showing the presence of both intra and extracellular AgNP. These images were collected after the RBCs were post-washed and dispersed in a 5% glucose solution.

It was observed that as the cell moves into focus, so do AgNPs. As more slices of the cell were taken, other NPs come into focus. If the NPs were above or below the cell, they would be in focus in the earliest and latest images that were collected when the cell is slightly out of focus.

The presence of both intracellular and extracellular AgNPs was made clear with Cytoviva, but to draw conclusions about the specific molecular interactions taking place, Raman spectroscopy was needed.

Red blood cells have a lot of characteristic Raman peaks which can be seen in the raw AgNP exposed RBC spectrum below (Figure 3.10). The assignments for each characteristic peak are shown in Table 3.7. In this raw spectrum, it is difficult to distinguish all of the peaks, especially in the spin-state marker region (1500-1650 $cm^{-1}$) which gives information about the type of hemoglobin present. Thus, all spectra were averaged, baseline corrected and normalized to the 1550 $cm^{-1}$ shift. Figure 3.10 also shows averaged spectra for aqueous control solutions, citrate and glucose (N=3). These solutions had a few peaks with very low intensities (>1000 cts).

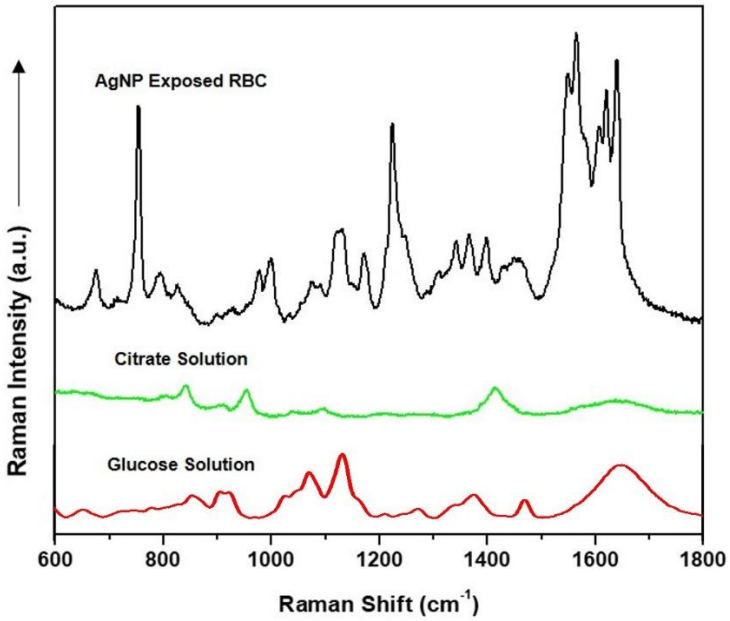


**Figure 3.10** Raman spectra of a 5% glucose solution, 1% citrate solution and AgNP exposed RBCs prior to baseline correction or normalization.

Vehicle control and AgNP exposed RBCs were washed following incubation and prepared for analysis. Similar to the Cytoviva results, the vehicle control cells appeared to have normal shape and size (Figure 3.11a). Obvious membrane damage could be seen in the AgNP exposed RBCs by their shriveled and contorted shapes. The AgNP exposed RBCs were stored in a 5% glucose solution at 4°C overnight and after approximately 24 hours, irreversible agglutination occurred. When RBCs are stored without anticoagulant solutions, they aggregate. Aggregation of the vehicle control cells took place after 24 hours, but the RBCs were easily separated with gentle agitation of the solution. However, the AgNP exposed RBCs did not redisperse even after the 5% glucose solution containing the cells was vortexed. It was suspected that interactions between extracellular AgNPs and surrounding cells formed these large clusters of RBCs that can be seen in

Figure 3.11c. These large cell aggregates would likely not form *in vivo* due to blood pressure and sheer forces in capillaries, but their formation attests to the strength of the AgNP interaction with the cell membrane.

Thirty spectra were collected of the vehicle control cells, AgNP exposed RBCs and RBC clusters. The spectra were averaged, baseline corrected and normalized to the 1550 $cm^{-1}$ peak. In the spontaneous Raman spectra of the vehicle control RBCs, all the typical oxyhemoglobin peaks corresponding to Fe in the low spin state (S=0) were observed. Again, each peaks assignment to hemoglobin or cellular components can be found in Table 3.7. In Figure 3.11d, the averaged Raman spectra of the AgNP exposed and clustered RBCs from three separate incubation trials are also presented (N=30). Ten percent of the AgNP exposed RBC spectra showed increased intensities, SERS enhancement, when compared to the average intensities observed in the vehicle control spectra. The lack of significant SERS enhancement in these spectra is due to the small size of the AgNPs. The colloid used in this experiment only showed significant SERS enhancement of R6G after induced aggregation. However, 50% of the RBC cluster spectra showed significant SERS enhancement confirming the presence of extracellular AgNP aggregates.

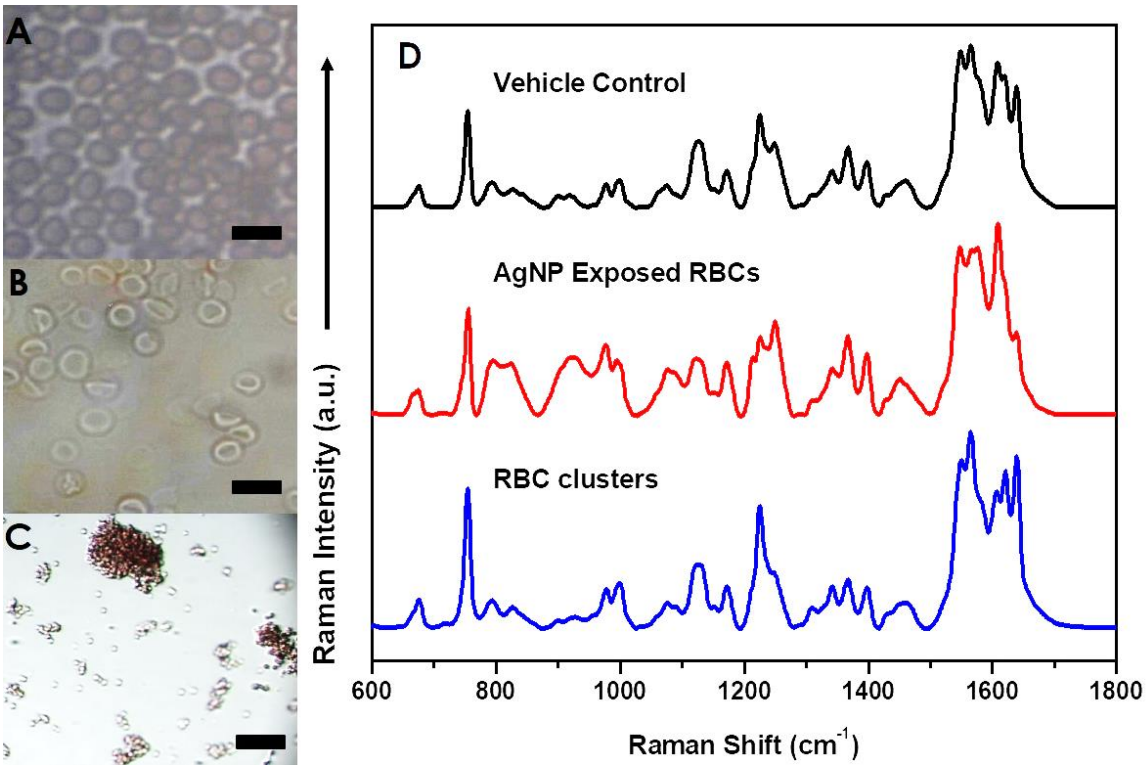


**Figure 3.11** Raman micrographs of the A) vehicle control B) post-washed RBC sample C) RBC cluster and D) their corresponding averaged Raman spectra (N=30). Scale bars represent A) 10 µm B) 10 µm and C) 40 µm.

When compared to the average vehicle control spectrum, the average AgNP exposed RBC and RBC cluster spectra showed several changes. The peak areas for the shifts that showed significant changes are highlighted in Table 3.8. These peak areas were used to calculate percent difference between the AgNP exposed RBCs or RBC clusters and the vehicle control RBCs. One of the most obvious differences is the presence of a very broad peak with a maximum at 921 $cm^{-1}$ in the AgNP exposed spectra. The RBC cluster spectrum also has a broader peak at 927 $cm^{-1}$. The manifestation of this peak in both spectra indicates the interaction of AgNPs with amino acids in the hemoglobin protein, and/or proteins on the cell membrane.[42] The shift in the peak maxima from 1460 to 1452 $cm^{-1}$ would also suggest the adhesion of AgNP to lipids on the cell membrane.[42]

Another noticeable difference is the 87±18% and 205±17% signal enhancement in the AgNP exposed RBCs of the 793 and 826 $cm^{-1}$ peaks, respectively. These peaks are assigned to the breathing of pyrrole and out of plane deformation of the adjoining methine group. Some of the increase peak area of the 826 $cm^{-1}$ could be attributed to overlap of the citrate peak at 840 $cm^{-1}$. Regardless, the enhancement of these peaks shows NP interaction the hemoglobin protein which suggests the presence of intracellular AgNPs.

It is possible that electrostatic forces between the negatively charged citrate capped AgNP and the positive iron in heme would orient the NP in such a way that interaction with the pyrrole ring would be probable. If a AgNP was interacting with the coordinated iron atom, the protein would suffer structural changes or denaturation and oxygen binding would be unlikely. This is just conjecture; further studies would need to be performed in order to confirm these presumptions. Structural changes or denaturation of the hemoglobin protein might explain the contorted cell shape observed in Figure 3.10b.

**Table 3.7** Tentative assignments of Raman vibrational bands observed in hemoglobin and molecules in RBCs. Peaks denoted with [a] correspond to reference 42, [b] correspond to reference 61, [c] correspond to reference 62, and [d] correspond to reference 63. Abbreviation: pyr, pyrrole; deform, deformation; sym, symmetric; asym, asymmetric; Trp, tryptophan; ν, valence; δ, in plane deformation; ϒ, out of plane deformation

| Raman Shift ($cm^{-1}$) | Vehicle Control | AgNP Exposed RBCs | RBC Clusters | Assignment |
|---|---|---|---|---|
| 674 | 675 | 674 | 675 | $\delta(\text{pyr deform})_{sym}$[b] |
| 715 | | | 717 | $\text{Pyr fold}_{asym}$[b] |
| 751/757 | 754 | 755 | 754 | ν(pyr breathing)[b] |
| 799 | 793 | 796 | 794 | ν(pyr breathing)[a] |
| 828 | 826 | 824 | 828 | $\Upsilon(C_mH)$[a] |
| 897 | 900 | | 899 | Uracil/Thymine[d] |
| 919 | 919 | | | $\Upsilon(=C_bH_2)$[b] |
| 924 | | 921 | 927 | Amino Acids: C-$COO^-$ stretch[a] |
| 977 | 977 | 977 | 978 | $\delta(\text{pyr deform})_{asym}$[c] and/or $\Upsilon(=C_bH_2)_{sym}$[c] |
| 996 | 999 | 996 | 1000 | $\nu(C_\beta C_1)_{asym}$[c] |
| 1076 | 1075 | 1076 | 1076 | Cytosine/Uracil[d] |
| 1090 | | 1089 | 1091 | $\nu(C_\beta C_1)_{asym}$[c] |
| 1123 | | 1123 | 1122 | $\nu(\text{pyr half-ring})_{sym}$[c] |
| 1131 | 1126 | | 1130 | $\nu(\text{pyr half-ring})_{asym}$[b] |
| 1153 | 1151 | 1150 | 1152 | $\nu(C_\beta C_1)_{sym}$[b] |
| 1172 | 1172 | 1172 | 1173 | $\nu(\text{pyr half-ring})_{asym}$[a] |
| 1212 | | 1214 | | $\delta(C_mH)$[a] |
| 1226 | 1225 | 1226 | 1225 | $\delta(C_mH)$[a] |
| 1248 | 1249 | 1250 | 1249 | $\delta(C_mH)$[c] |
| 1306 | 1309 | 1308 | 1309 | $\delta(C_mH)$[c] |
| 1341 | 1342 | 1342 | 1342 | $\nu(\text{pyr half-ring})_{sym}$[b] |
| 1366 | 1367 | 1367 | 1367 | $\nu(\text{pyr half-ring})_{sym}$[c] |
| 1398 | 1398 | 1398 | 1399 | ν(pyr quarter-ring)[c] |
| 1428 | 1428 | 1428 | 1430 | $\nu(C_\alpha C_m)_{sym}$[c] |
| 1452 | | 1452 | | Lipids: $\delta(CH_2/CH_3)$[a] |
| 1461 | 1460 | | 1460 | Adenine/Guanine[d] |
| 1550 | 1549 | 1547 | 1550 | $\nu(C_\beta C_\beta)$[a] Proteins, lipids: amide II, Trp[a] |
| 1563 | 1566 | 1567 | 1566 | $\nu(C_\beta C_\beta)$[c] |
| 1580 | 1580 | 1576 | 1583 | $\nu(C_\alpha C_m)_{asym}$[c] |
| 1608 | 1609 | 1609 | 1607 | $\nu(C_\alpha C_m)_{asym}$[c] |
| 1618 | 1620 | | 1620 | $\nu(C_\alpha{=}C_b)$[c] |
| 1638 | 1640 | 1639 | 1640 | $\nu(C_\alpha C_m)_{asym}$[c] |

In both the AgNP exposed and clustered RBCs, SERS enhancement within the cell causes the appearance of shifts at 1090 and 1123 $cm^{-1}$. Corresponding to the vibrations of the double bonded carbons and asymmetric half-ring stretch of pyrrole, the interaction of heme with AgNPs is further supported. The conformational change from the R to T state in deoxyhemoglobin causes a change in the deformation angle of the methine group.[62] This causes the vibrational frequency in the C-H to shift from 1226 to 1214 $cm^{-1}$.[64] The 36±4% decrease in peak area of the 1226 $cm^{-1}$ combined with the presence of the 1214 $cm^{-1}$ shift in the AgNP exposed RBCs indicates the formation of deoxyhemoglobin. The most prevalent differences between the control and the AgNP treated RBCs occur in the spin-state marker region of heme from 1500 to 1650 $cm^{-1}$.

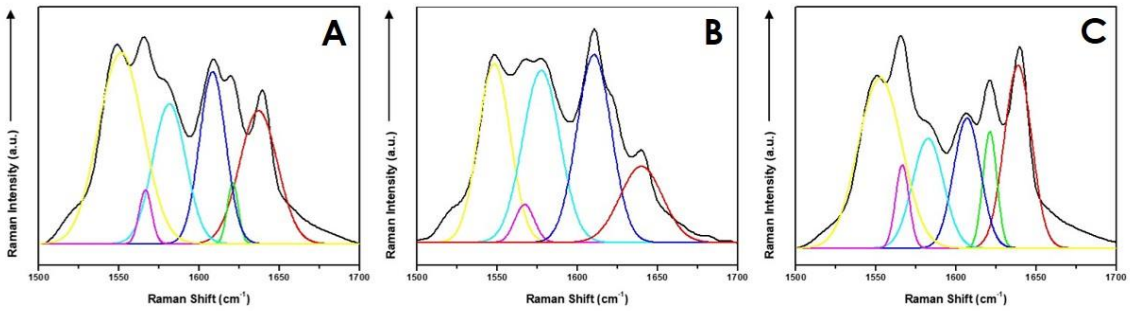


**Figure 3.12** Sample plots showing the deconvolution of peaks with Raman shifts ranging from 1550-1650 $cm^{-1}$ for the A) vehicle control, B) AgNP exposed RBCs and C) the RBC clusters.

In the AgNP exposed RBCs, there was a 38±20% increase in the 1609 $cm^{-1}$ shift. Additionally, there was diminishment of 1620 $cm^{-1}$ and a 48±12% decrease in the 1640 $cm^{-1}$ peak. The 1609 $cm^{-1}$ peak is assigned to an asymmetric stretch of $\nu(C_\alpha C_m)$. The increase in this peak area means Fe is in a high spin state (S=2) which indicates the

presence of deoxyhemoglobin.[62] This is confirmed by the decrease in area of oxyhemoglobin shifts at 1620 and 1640 $cm^{-1}$.

An interesting increase of 204±151% of the oxyhemoglobin peak in the averaged RBC cluster spectrum is likely the result of the SERS enhancement from extracellular AgNP aggregates. There are large uncertainties in the peak areas for 1609 and 1620 $cm^{-1}$ due to the fact that some spectra showed the presence of oxyhemoglobin while others showed deoxyhemoglobin. Even though specific shifts in the spectra showed variance, the overall intensities increased by a factor up to 5 times those of the vehicle control cells. The average max intensity of the vehicle control cells was 3,750 A.U. compared to 19,250 A.U. of the RBC clusters. This large SERS enhancement confirms the presence of hotspots between extracellular AgNPs.

**Table 3.8** Peak areas for various Raman shifts observed in the vehicle control, AgNP exposed RBCs and RBC clusters.

| Raman Shift ($cm^{-1}$) | Vehicle Control | AgNP Exposed RBCs | RBC Clusters |
|---|---|---|---|
| 793 | 3.1 ± 0.2 | 5.8 ± 0.5 | 4.2 ± 0.2 |
| 826 | 4.4 ± 0.2 | 13.4 ± 0.6 | 3.7 ± 0.2 |
| 1214 | - | 2.4 ± 0.3 | - |
| 1226 | 11.6 ± 0.3 | 7.4 ± 0.5 | 13.2 ± 0.5 |
| 1609 | 16.8 ± 3 | 23.3 ± 1 | 15.9 ± 7 |
| 1620 | 2.4 ± 1 | - | 7.3 ± 3 |
| 1640 | 18.4 ± 1 | 9.5 ± 2 | 22.7 ± 0.8 |

The enhancement of shifts corresponding to pyrrole stretches prove that intracellular AgNPs are within hemoglobin and causing structural changes to the protein. The presence of numerous deoxyhemoglobin peaks are likely a result of both intracellular and

extracellular AgNPs. Intracellular AgNPs are attracted to and interact with iron ions causing a high spin state or T-state conformation in heme. Extracellular AgNPs could have damaged the cell membrane or blocked the band 3 transmembrane protein which regulates the pH of the cell. Both interactions would cause a change in the intracellular pH which could have caused the deoxygenation of hemoglobin.[41]

## 4. CONCLUSION

This study aimed to determine the uptake, distribution and molecular interaction of AgNPs with human red blood cells. Citrate capped AgNPs were synthesized and filtered to achieve a pure colloid of spherical particles 5-10 nm in diameter. Packed RBCs were washed with PBS prior to incubation with the filtered AgNPs in a 5% glucose solution for 1 hour to achieve a hematocrit of 32±3%. Three post-washes with glucose were necessary to remove unbound AgNPs for quantification on GFAAS. The post-washed cells were also analyzed via Cytoviva hyperspectral microscopy and Raman spectroscopy.

The uptake of AgNPs adhered to and within the RBCs was quantified on GFAAS and found to be 48±5%. Along with the makeup of the cell membrane, the size and coating of the AgNPs contributed to the uptake. CytoViva images and hyperspectral results demonstrated the strong adhesion of AgNPs to the cell membrane along with the existence of intracellular AgNPs. About 70% of the AgNPs that were quantified with GFAAS were adhered to the cell membrane and 30% were distributed within the cells. Many cells exposed to AgNPs showed obvious membrane damage indicated by the distorted shape. The CytoViva 3D function was used to confirm the presence of AgNPs within the cytoplasm of RBCs. CytoViva was also a useful tool in determining the aggregation state of both the intracellular and extracellular AgNPs, neither of which seemed to aggregate or grow in size during the one-hour incubation. However, after 24

hours of storage at 4°C in 5% glucose solution, agglutination of the RBCs occurred. The extreme Raman signal enhancement of over 400% in the RBC cluster spectra suggested that extracellular AgNP aggregates were forming between multiple RBCs. Averaged Raman spectra of the AgNP exposed RBCs showed interaction with heme as well as decreases in oxyhemoglobin and enhanced deoxyhemoglobin peaks. The deoxygenation of heme could be the result of direct interaction with intracellular AgNPs, and/or cell membrane damage or blockage of membrane proteins caused by extracellular AgNPs.

The results of this study show that there could be serious health concerns if AgNPs continue to be used in biomedical technologies and exposed to the cardiovascular system. The high percent uptake and strong membrane interactions mean AgNPs would remain concentrated in the circulatory system rather than being dispersed or excreted. Eventually, the release of toxic silver ions from the adsorbed AgNPs into the blood stream could cause necrosis of not only RBCs, but also white blood cells which are a vital part of the immune system. Intracellular interactions with hemoglobin could cause a lack of oxygen delivery to major organs which could lead to a wide array of health issues.

It is important that future experiments be performed to quantify the uptake of AgNPs with various sizes and coatings in human RBCs to further determine which factors have the largest effect. The molecular interaction of larger NPs with the cell membrane and their effects on hemoglobin should also be studied via Raman spectroscopy. *In vitro* studies provide valuable results about interactions at a small scale, however more work should be done *in vivo* to truly determine the large-scale effects.

## REFERENCES


1. Consumer Products Inventory. http://www.nanotechproject.org/cpi/products/ (accessed Oct 12, 2017).

2. National Science Foundation - Where Discoveries Begin. https://www.nsf.gov/news/news_summ.jsp?cntn_id=130586 (accessed Oct 11, 2017).

3. Kessler, R. Engineered Nanoparticles in Consumer Products: Understanding a New Ingredient. *Environ. Health Perspect.* **2011**, *11*9, A120-A125.

4. Ge, L.; Li, Q.; Wang, M.; Ouyang, J.; Li, X.; Xing, M. M. Q. Nanosilver particles in medical applications: synthesis, performance, and toxicity. *International Journal of Nanomedicine* **2014**, 9, 2399-2407.

5. Zhang, W.; Yao, Y.; Sullivan, N.; Chen, Y. Modeling the Primary Size Effects of Citrate-Coated Silver Nanoparticles on Their Ion Release Kinetics. *Environ. Sci. Technol.* **2011**, *4*5, 4422-4428.

6. Sibbald, R. G.; Contreras-Ruiz, J.; Coutts, P.; Fierheller, M.; Rothman, A.; Woo, K. Bacteriology, inflammation, and healing: a study of nanocrystalline silver dressings in chronic venous leg ulcers. *Adv. Skin Wound Care* **2007**, *2*0, 549-558.

7. Haes; J., A.; Hall; P., W.; Chang; L.; Klein; L., W.; Duyne, V.; P., R. A Localized Surface Plasmon Resonance Biosensor: First Steps toward an Assay for Alzheimer's Disease. *Nano Letters* **2004**, 4, 1029-1034.

8. Potara, M.; Bawaskar, M.; Simon, T.; Gaikwad, S.; Licarete, E.; Ingle, A.; Banciu, M.; Vulpoi, A.; Astilean, S.; Rai, M. Biosynthesized silver nanoparticles performing as biogenic SERS-nanotags for investigation of C26 colon carcinoma cells. *Colloids and Surfaces B: Biointerfaces* **2015**, *13*3, 296-303.

9. Platas-Iglesias, C.; Benyettou, F.; Rezgui, R.; Jaber, T.; Blumer, K.; Magzoub, M.; Trabolsi, A.; Ravaux, F.; Jouiad, M.; Motte, L.; Olsen, J. -.; Platas-Iglesias, C. Synthesis of silver nanoparticles for the dual delivery of doxorubicin and alendronate to cancer cells. *Journal of Materials Chemistry B* **2015**, 3, 7237-7245.

10. Venugopal, K.; Rather, H. A.; Rajagopal, K.; Shanthi, M. P.; Sheriff, K.; Illiyas, M.; Rather, R. A.; Manikandan, E.; Uvarajan, S.; Bhaskar, M.; Maaza, M. Synthesis of silver nanoparticles (Ag NPs) for anticancer activities (MCF 7 breast and A549 lung cell lines) of the crude extract of Syzygium aromaticum. *Journal of Photochemistry & Photobiology, B: Biology* **2017**, *167*, 282-289.

11. Daraio, C.; Jin, S. Synthesis and Patterning Methods for Nanostructures Useful for Biological Applications. *Nanotechnology for Biology & Medicine* **2012**, 27.

12. Kumar, N.; Kumbhat, S. Nanomaterials: General Synthetic Approaches. In *Essentials in Nanoscience and Nanotechnology*John Wiley & Sons, Inc: 2016; pp 29-76.

13. Sau, T. K.; Rogach, A. L. *Complex-shaped metal nanoparticles. [electronic resource] : bottom-up syntheses and applications;* Weinheim : Wiley-VCH, c2012: 2012 .

14. Pacioni, N. L.; Borsarelli, C. D.; Rey, V.; Veglia, A. V. Synthetic Routes for the Preparation of Silver Nanoparticles. In *Silver Nanoparticle Applications: In the Fabrication and Design of Medical and Biosensing Device*s; Alarcon, E. I., Griffith, M. and Udekwu, K. I., Eds.; Springer International Publishing: Cham, 2015; pp 13-46.

15. Bonor, J.; Reddy, V.; Akkiraju, H.; Dhurjati, P.; Nohe, A. Synthesis and Characterization of L-Lysine Conjugated Silver Nanoparticles Smaller Than 10 nM. *Adv Sci Eng Med* **2014**, 6, 942-947.

16. Abdollahi, Y.; Shameli, K.; Mahdavi, M.; Jahangirian, H.; Seyed, D. J.; Sedaghat, S.; Shabanzadeh, P.; Mansor, B. A. Synthesis and Characterization of Polyethylene Glycol Mediated Silver Nanoparticles by the Green Method. *International Journal of Molecular Sciences, Vol 13, Iss 6, Pp 6639-6650 (2012)* **2012**, 6639.

17. Rogers, K. R.; Navratilova, J.; Stefaniak, A.; Bowers, L.; Knepp, A. K.; Al-Abed, S.; Potter, P.; Gitipour, A.; Radwan, I.; Nelson, C.; Bradham, K. D. Characterization of engineered nanoparticles in commercially available spray disinfectant products advertised to contain colloidal silver. *Sci. Total Environ.* **2018**, *619-62*0, 1375-1384.

18. Lee, P. C.; Meisel, D. Adsorption and surface-enhanced Raman of dyes on silver and gold sols. *J. Phys. Chem.* **1982**, *8*6, 3391-3395.

19. Creighton, J. A.; Blatchford, C. G.; Albrecht, M. G. Plasma resonance enhancement of Raman scattering by pyridine adsorbed on silver or gold sol particles of size comparable to the excitation wavelength. *Journal of the Chemical Society, Faraday Transactions 2: Molecular & Chemical Physics* **1979**, *7*5, 790.

20. Tejamaya, M.; Roemer, I.; Merrifield, R. C.; Lead, J. R. Stability of Citrate, PVP, and PEG Coated Silver Nanoparticles in Ecotoxicology Media. *Environ. Sci. Technol.* **2012**, *4*6, 7011-7017.

21. Bastus, N.; Puntes, V.; Piella, J.; Bastus, N. G.; Merkoci, F.; Piella, J.; Puntes, V. Synthesis of Highly Monodisperse Citrate-Stabilized Silver Nanoparticles of up to 200 nm: Kinetic Control and Catalytic Properties. *Chemistry of Materials* **2014**, *2*6, 2836-2846.

22. Agnihotri, S.; Mukherji, S.; Agnihotri, S.; Mukherji, S.; Mukherji, S. Size-controlled silver nanoparticles synthesized over the range 5-100 nm using the same protocol and their antibacterial efficacy. *RSC Advances* **2014**, 4, 3974-3983.

23. Mishra, M. P.; Padhy, R. N. Antibacterial activity of green silver nanoparticles synthesized from Anogeissus acuminata against multidrug resistant urinary tract infecting bacteria in vitro and host-toxicity testing. *Journal of Applied Biomedicine (Elsevier Inc. )* **2018**, *1*6, 120-125.

24. Khalandi, B.; Asadi, N.; Milani, M.; Davaran, S.; Abadi, A. J. N.; Abasi, E.; Akbarzadeh, A. A Review on Potential Role of Silver Nanoparticles and Possible Mechanisms of their Actions on Bacteria. *Drug Res (Stuttg)* **2017**, *6*7, 70-76.

25. Han, J.; Gurunathan, S.; Jeong, J.; Choi, Y.; Kwon, D.; Park, J.; Kim, J. Oxidative stress mediated cytotoxicity of biologically synthesized silver nanoparticles in human lung epithelial adenocarcinoma cell line. *Nanoscale Research Letters* **2014**, 9, 1-14.

26. AshaRani, P. V.; Low, K. M.; Hande, M. P.; Valiyaveettil, S. Cytotoxicity and genotoxicity of silver nanoparticles in human cells. *ACS Nano* **2009**, 3, 279-290.

27. Zhang, X.; Shen, W.; Gurunathan, S. Silver Nanoparticle-Mediated Cellular Responses in Various Cell Lines: An in Vitro Model. *International Journal of Molecular Sciences* **2016**, *17*.

28. Wang, E.; Huang, Y.; Du, Q.; Sun, Y. Silver nanoparticle induced toxicity to human sperm by increasing ROS (reactive oxygen species) production and DNA damage. *Environ. Toxicol. Pharmacol.* **2017**, *5*2, 193-199.

29. Lynch, I.; Dawson, K. A.; Luch, A.; Reidy, B.; Haase, A. Mechanisms of Silver Nanoparticle Release, Transformation and Toxicity: A Critical Review of Current Knowledge and Recommendations for Future Studies and Applications. *Materials, Vol 6, Iss 6, Pp 2295-2350 (2013)* **2013**, 2295.

30. Ma, W.; Jing, L.; Valladares, A.; Mehta, S. L.; Wang, Z.; Li, P. A.; Bang, J. J. Silver nanoparticle exposure induced mitochondrial stress, caspase-3 activation and cell death: amelioration by sodium selenite. *Int J Biol Sci* **2015**, *1*1, 860-867.

31. Singh, R. P.; Ramarao, P. Cellular uptake, intracellular trafficking and cytotoxicity of silver nanoparticles. *Toxicol. Lett.* **2012**, *213*, 249-259.

32. Shang, L.; Nienhaus, G. U.; Shang, L.; Nienhaus, K.; Nienhaus, G. U. Engineered nanoparticles interacting with cells: size matters. *Journal of Nanobiotechnology* **2014**, *12*.

33. Tang, J.; Xiong, L.; Wang, S.; Wang, J.; Liu, L.; Li, J.; Wan, Z.; Xi, T. Influence of silver nanoparticles on neurons and blood-brain barrier via subcutaneous injection in rats. *Appl. Surf. Sci.* **2008**, *25*5, 502-504.

34. Kim, Y. S.; Kim, J. S.; Cho, H. S.; Rha, D. S.; Kim, J. M.; Park, J. D.; Choi, B. S.; Lim, R.; Chang, H. K.; Chung, Y. H.; Kwon, I. H.; Jeong, J.; Han, B. S.; Yu, I. J. Twenty-eight-day oral toxicity, genotoxicity, and gender-related tissue distribution of silver nanoparticles in Sprague-Dawley rats. *Inhal. Toxicol.* **2008**, *2*0, 575-583.

35. Shrivastava, S.; Bera, T.; Singh, S. K.; Singh, G.; Ramachandrarao, P.; Dash, D. Characterization of antiplatelet properties of silver nanoparticles. *ACS Nano* **2009**, 3, 1357-1364.

36. Valiyaveettil, S.; Gong, Z.; Asharani, P. V.; Valiyaveettil, S.; Wu, Y. L.; Gong, Z. Toxicity of silver nanoparticles in zebrafish models. *Nanotechnology* **2008**, *1*9.

37. Fenske, M.; Baumgartner, W.; Muth-Koehne, E.; Sonnack, L.; Fenske, M.; Schlich, K.; Hund-Rinke, K.; Schaefers, C.; Hischen, F.; Baumgartner, W. The toxicity of silver nanoparticles to zebrafish embryos increases through sewage treatment processes. *Ecotoxicology* **2013**, *22*, 1264-1277.

38. Gahan, P. B. Life: the science of biology (7th edn) W. K. Purves, D. Sadava, G. H. Orians and H. C. Heller, W. H. Freeman & Co, 1121 pp., ISBN 0-7167-9856-5 (2004). *Cell Biochemistry & Function* **2005**, *2*3, 221.

39. Kim, J.; Lee, H.; Shin, S. Advances in the measurement of red blood cell deformability: A brief review. *Journal of Cellular Biotechnology* **2015**, 1, 63.

40. Chen, L. Q.; Fang, L.; Ling, J.; Ding, C. Z.; Kang, B.; Huang, C. Z. Nanotoxicity of Silver Nanoparticles to Red Blood Cells: Size Dependent Adsorption, Uptake, and Hemolytic Activity. *Chem. Res. Toxicol.* **2015**, *2*8, 501-509.

41. Bankapur, A.; Barkur, S.; Chidangil, S.; Mathur, D. A Micro-Raman Study of Live, Single Red Blood Cells (RBCs) Treated with $AgNO_3$ Nanoparticles. *PLoS ONE* **2014**, 9, 1-10.

42. Drescher, D.; Buechner, T.; Kneipp, J.; McNaughton, D. SERS reveals the specific interaction of silver and gold nanoparticles with hemoglobin and red blood cell components. *Physical Chemistry Chemical Physics* **2013**, *1*5, 5364-5373.

43. Wan, Y.; Guo, Z.; Jiang, X.; Fang, K.; Lu, X.; Zhang, Y.; Gu, N. Quasi-spherical silver nanoparticles: Aqueous synthesis and size control by the seed-mediated Lee–Meisel method. *J. Colloid Interface Sci.* **2013**, *39*4, 263-268.

44. Park, K.; Lee, Y. The Stability of Citrate-Capped Silver Nanoparticles in Isotonic Glucose Solution for Intravenous Injection. *Journal of Toxicology & Environmental Health: Part A* **2013**, *7*6, 1236-1245.

45. Monahan, J. L.; Weaver, K. M.; Meyerhoefer, A. J.; Markopolous, M. M.; Arnold, Z. S.; Pavel, I. E.; Trefry, J. C.; Wooley, D. P. Size Selection and Concentration of Silver Nanoparticles by Tangential Flow Ultrafiltration for SERS-Based Biosensors. *J. Am. Chem. Soc.* **2010**, *132*, 10970-10972.

46. Perrone, I.; Ferreira Torres, J. K.; Stephani, R.; Tavares, G. M.; de Carvalho, A. F.; Perrone, I. T.; Rocha, d. A.; Almeida, M. R.; Cappa, d. O.; Bueno Costa, R. G.; Schuck, P. Technological aspects of lactose-hydrolyzed milk powder. *Food Res. Int.* **2017**, *101*, 45-53.

47. Nonoyama, A.; Potter, R. L.; Garcia-Lopez, A.; Garcia-Rubio, L.; Leparc, G. F. Hypochromicity in red blood cells: an experimental and theoretical investigation. *Biomedical Optics Express* **2011**, *2*, 2126-2143.

48. Uppal, S.; Kumar, A.; Shandilya, M.; Mukhi, N.; Singh, A. K.; Kateriya, S.; Kaur, J.; Kundu, S. Penta- and hexa-coordinate ferric hemoglobins display distinct pH titration profiles measured by Soret peak shifts. *Anal. Biochem.* **2016**, *510*, 120-128.

49. Hanson, E. K.; Ballantyne, J. A Blue Spectral Shift of the Hemoglobin Soret Band Correlates with the Age (Time Since Deposition) of Dried Bloodstains. *PLoS ONE* **2010**, *5*, 1-11.

50. Wood, B.; Hammer, L.; Davis, L.; McNaughton, D. Raman microspectroscopy and imaging provides insights into heme aggregation and denaturation with human erythrocytes*; J. Biomed. Opt.* **2005**; Vol. 10, pp 14005.

51. Understanding Blood Counts. *https://www.lls.org/managing-your-cancer/lab-and-imaging-tests/understanding-blood-counts* (accessed 7/24, 2018).

52. Walker, H. K.; Hall, W. D.; Hurst, J. W. Clinical Methods: The History, Physical, and Laboratory Examinations. **1990**.

53. Paluri, S. L. A.; Ryan, J. D.; Lam, N. H.; Sizemore, I. E.; Nepal, D. Analytical-Based Methodologies for Examining the In Vitro Absorption, Distribution, Metabolism, and Elimination (ADME) of Silver Nanoparticles. *SMALL* **2017**, *13*.

54. Wood, B. Raman microspectroscopy and imaging provides insights into heme aggregation and denaturation within human erythrocytes. *J. Biomed. Opt.* **2005**, *10*.

55. Liu, J.; Yu, S.; Chao, J.; Sun, J.; Yin, Y.; Liu, J.; Jiang, G. Quantification of the Uptake of Silver Nanoparticles and Ions to HepG2 Cells. *Environ. Sci. Technol.* **2013**, *47*, 3268-3274.

56. Freese, C.; Uboldi, C.; Gibson, M. I.; Unger, R. E.; Weksler, B. B.; Romero, I. A.; Couraud, P.; Kirkpatrick, C. J. Uptake and cytotoxicity of citrate-coated gold nanospheres: Comparative studies on human endothelial and epithelial cells. *Part Fibre Toxicol* **2012**, *9*, 23-23.

57. Hendriks, A. J.; Kettler, K.; Hendriks, A. J.; Krystek, P.; Giannakou, C.; de Jong, W. H. Exploring the effect of silver nanoparticle size and medium composition on uptake into pulmonary epithelial 16HBE14o-cells. *Journal of Nanoparticle Research* **2016**, *18*, 1-11.

58. Ghitescu, L.; Fixman, A. Surface Charge Distribution on the Endothelial Cell of Liver Sinusoids. *J. Cell Biol.* **1984**, 639.

59. Bhat, A.; Huan, K.; Cooks, T.; Boukari, H.; Lu, Q. Probing Interactions between AuNPs/AgNPs and Giant Unilamellar Vesicles (GUVs) Using Hyperspectral Dark-field Microscopy. *International Journal of Molecular Sciences* **2018**, *19*, 1-14.

60. Conti, M.; Scanferlato, R.; Louka, M.; Sansone, A.; Marzetti, C.; Ferreri, C. Building up spectral libraries for mapping erythrocytes by hyperspectral dark field microscopy. *Biomedical Spectroscopy & Imaging* **2016**, *5*, 175-184.

61. Hu, S.; Smith, K. M.; Spiro, T. G. Assignment of Protoheme Resonance Raman Spectrum by Heme Labeling in Myoglobin. *J. Am. Chem. Soc.* **1996**, *118*, 12638-12646.

62. Wood, B. R.; Caspers, P.; Puppels, G. J.; Pandiancherri, S.; McNaughton, D. Resonance Raman spectroscopy of red blood cells using near-infrared laser excitation. *Analytical & Bioanalytical Chemistry* **2007**, *387*, 1691-1703.

63. Madzharova, F.; Heiner, Z.; Guehlke, M.; Kneipp, J. Surface-Enhanced Hyper-Raman Spectra of Adenine, Guanine, Cytosine, Thymine, and Uracil. *Journal of Physical Chemistry C* **2016**, *120*, 15415-15423.

64. Atkins, C. G.; Buckley, K.; Turner, R. F. B.; Blades, M. W. Raman Spectroscopy of Blood and Blood Components. *Appl. Spectrosc.* **2017**, *71*, 767-793.